Physics – Uspekhi **64** (9) 923 – 946 (2021)

REVIEWS OF TOPICAL PROBLEMS PACS numbers: **72.70.+m, 78.67.–n**

Theory of optically detected spin noise in nanosystems

D S Smirnov, V N Mantsevich, M M Glazov

DOI: https://doi.org/10.3367/UFNe.2020.10.038861

Contents

Abstract. The theory of spin noise in low-dimensional systems and bulk semiconductors is reviewed. Spin noise is usually detected by optical means continuously measuring the rotation angle of the polarization direction of a probe beam passing through a sample. Spin noise spectra yield rich information about the spin properties of the system, for example, *g*-factors of the charge carriers, spin relaxation times, parameters of the hyperfine interaction, spin-orbit coupling constants, frequencies and widths of the optical resonances. The review describes basic models of spin noise, methods to theoretically describe it, and their relation to experimental results. We also discuss the relation between spin noise spectroscopy and strong and weak quantum measurements, as well as spin flip Raman scattering, and analyze similar effects, including manifestations of the charge, current, and valley polarization fluctuations in the optical response. Possible directions for further development of spin noise spectroscopy are outlined.

Keywords: spin noise, spin correlation functions, nanosystems, quantum dots, nanowires, quantum wells, spin Faraday effect, hyperfine interaction, exchange interaction, spin-orbit coupling

D S Smirnov [1, 3, a], **V N Mantsevich** [2, b], **M M Glazov** [1, c]
[1] Ioffe Institute,
ul. Politekhnicheskaya 26, 194021 Saint-Petersburg,
Russian Federation
[2] Lomonosov Moscow State University,
Leninskie gory, 119991 Moscow, Russian Federation
[3] Spin Optics Laboratory, St. Petersburg State University,
ul. Ulyanovskaya 1, 198504 Saint-Petersburg, Russian Federation
E-mail: [a] smirnov@mail.ioffe.ru, [b] vmantsev@gmail.com,
[c] glazov@coherent.ioffe.ru

Received 6 July 2020
Uspekhi Fizicheskikh Nauk **191** (9) 973 – 998 (2021)
Translated by V N Mantsevich

1. Introduction

Studies of spin phenomena have formed a broad and rapidly developing branch of solid state physics since the beginning of the 21st century. Such rapid progress is related to, on the one hand, the prospects of realizing quantum methods for information processing and, on the other hand, the novel fundamental physics of spin phenomena which manifest themselves in condensed matter. Usually, the dynamics of electron and nuclear spin ensembles in semiconductors are studied via monitoring the response of the system to external perturbations, mainly, to alternating electric and magnetic fields. One can detect, using the polarization of emitted light and spin-Faraday and Kerr effects, i.e., the rotation of the probe beam polarization plane upon its transmission through the medium or its reflection from it, spin precession in external fields and spin relaxation resulting from the excitation of spin polarization, e.g., by circularly polarized light.

It is natural to ask a question regarding what one can learn about the spin dynamics from studies of the Faraday or Kerr rotation without any excitation of the system. Imminent fluctuations of electron spins, $\delta S_z(t)$ (see Fig. 1), result in a stochastic contribution to the Faraday rotation angle:

$$\delta\theta_{\rm F}(t) \propto \delta S_z(t)\,. \tag{1}$$

Here, z is the light propagation axis, and we assume that the retardation effects upon light transmission can be ignored. By definition, spin fluctuations are absent, on average, $\langle \delta S_\alpha(t)\rangle = 0$. Here, the angular brackets denote time averaging, namely,

$$\langle \delta S_\alpha(t)\rangle = \lim_{T\to\infty} \frac{1}{2T}\int_{-T}^{T} \delta S_\alpha(t)\,{\rm d}t, \quad \alpha = x, y, z\,, \tag{2}$$

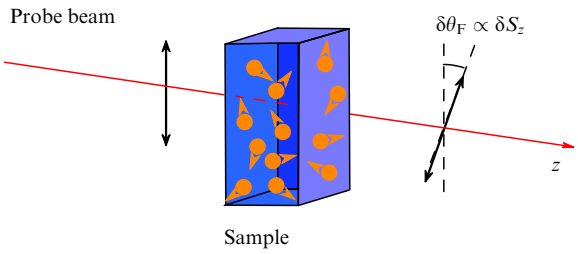

Figure 1. Illustration of spin fluctuations detection: z is the direction of linearly polarized light propagation, double arrows show orientation of linear polarization plane of the beam before and after its transmission through the medium with fluctuating spins.

where T is a macroscopic time which exceeds by far the spin precession period in external fields, times of spin decoherence and relaxation, etc. Spin fluctuations — spin noise — are characterized by correlation functions. Of prime interest are the second order correlation functions under the steady-state conditions [1], which are defined as follows:

$$\mathcal{C}_{\alpha\beta}(\tau) = \left\langle \delta S_\alpha(t+\tau)\, \delta S_\beta(t) \right\rangle . \tag{3}$$

In accordance with the general theory of fluctuations [2, 3], the averaging in Eqn (3) takes place over time t at a fixed difference between arguments τ. It is assumed in Eqn (3) that the quantity $\delta S_\alpha(t)$ is a classical one. Generally, one has to symmetrize quantum mechanical operators [2]

$$\mathcal{C}_{\alpha\beta}(\tau) = \left\langle \left\{ \delta\hat{S}_\alpha(t+\tau)\, \delta\hat{S}_\beta(t) \right\}_s \right\rangle , \tag{4}$$

where $\{\hat{A}\hat{B}\}_s = (\hat{A}\hat{B} + \hat{B}\hat{A})/2$, and the spin fluctuation operator $\delta\hat{S}_\alpha = \hat{S}_\alpha - \langle\hat{S}_\alpha\rangle$, with the angular brackets here denoting quantum mechanical averaging.

Owing to Eqn (1), the autocorrelation function of the Faraday rotation angles $\langle \delta\theta_F(t+\tau)\, \delta\theta_F(t)\rangle$ is directly proportional to the spin autocorrelation function $\mathcal{C}_{zz}(\tau)$. Thus, by observing fluctuations of the Faraday and Kerr rotation (as well as those of the ellipticity), one can directly measure the spin correlation function, which contains fundamental information on spin dynamics. In thermal equilibrium conditions, the functions $\mathcal{C}_{\alpha\beta}(\tau)$ are related via the fluctuation-dissipation theorem to the spin susceptibility of the system. E B Aleksandrov and V S Zapasskii were the first to detect spin fluctuations and, correspondingly, spin susceptibility in the noise of Faraday rotation in atomic gas vapors [4]. These experiments from the 1980s were reproduced at the beginning of the 2000s [5–7]. Later on, this method was applied to bulk semiconductors [8–10] and semiconductor nanosystems [11–14]. As a result, a novel area of spin dynamics studies, known as spin noise spectroscopy, was established [15–20].

To detect spin fluctuations superconducting interferometric devices [21, 22], scanning tunneling microscopy [23, 24], and magnetic resonance microscopy [25, 26] can be applied. However, in semiconductor systems, the optical methods described above are the most efficient.

In the next section of this review, a consistent description of the simplest methods for calculating spin fluctuations will be presented using, as an example, the spin precession in an external static magnetic field and isotropic spin relaxation, which is typical for bulk semiconductors. Next, in Sections 3–5, the specifics of the spin noise in, respectively, zero-, one-, and two-dimensional systems will be detailed. In Section 6, high order spin correlation functions will be described. Further, in Section 7, the capabilities of the spin noise spectroscopy technique, which go beyond measurements of spin correlators, will be described. The concluding Section 8 contains a summary and description of prospects for further development of the spin fluctuation theory in semiconductors.

2. Methods of spin noise spectrum calculations

2.1 Methods of the fluctuation theory

Let us consider fluctuations of a single electron spin $\delta\mathbf{s}(t)$ in a static magnetic field $\mathbf{B}$, which is characterized by a Larmor frequency $\boldsymbol{\Omega}_L = g\mu_B\mathbf{B}/\hbar$, where g is the g-factor and μ_B is the Bohr magneton. Spin correlation functions can be calculated by a number of methods. We present, first, the Langevin random forces approach based on the solution of the Bloch equation for spin fluctuation

$$\frac{\mathrm{d}\delta\mathbf{s}(t)}{\mathrm{d}t} + \frac{\delta\mathbf{s}(t)}{\tau_s} + \delta\mathbf{s}(t) \times \boldsymbol{\Omega}_L = \boldsymbol{\xi}(t) , \tag{5}$$

where τ_s is the phenomenological spin relaxation time, and $\boldsymbol{\xi}(t)$ are the random or Langevin forces. These fictitious forces are included on the right-hand side of Eqn (5) to support mean square fluctuations of the spin components

$$\left\langle \delta s_\alpha(t)\, \delta s_\beta(t) \right\rangle \equiv \left\langle \left\{ \delta\hat{s}_\alpha(t)\, \delta\hat{s}_\beta(t) \right\}_s \right\rangle = \frac{\delta_{\alpha\beta}}{4} . \tag{6}$$

This expression is given in the high-temperature limit, $k_B T \gg \hbar\Omega_L$, where magnetic field induced equilibrium polarization is negligible. Equation (6) directly follows from the spin operators definition. Since the Langevin forces are fictitious, i.e., they are not directly related to any real physical process, their correlation function must not contain any temporal scales, i.e., they reduce to the δ-function [2, 27–29]:

$$\left\langle \xi_\alpha(t)\xi_\beta(t+\tau) \right\rangle = \frac{1}{2\tau_s}\delta_{\alpha\beta}\delta(\tau) . \tag{7}$$

Solving Eqn (5), the spin correlators can be calculated in both the temporal and frequency representations. By definition,

$$\tilde{\mathcal{C}}_{\alpha\beta}(\omega) = (\delta s_\alpha \delta s_\beta)_\omega = \int_{-\infty}^{+\infty} \left\langle \delta s_\alpha(t+\tau)\, \delta s_\beta(t) \right\rangle \exp(\mathrm{i}\omega\tau)\, \mathrm{d}\tau . \tag{8}$$

In the coordinate frame x_1, y_1, z_1 with the axis $z_1 \parallel \boldsymbol{\Omega}_L$, we have [1, 30]

$$(\delta s_{z_1}^2)_\omega = \frac{\pi}{2} A(\omega) , \tag{9a}$$

$$(\delta s_{x_1}^2)_\omega = (\delta s_{y_1}^2)_\omega = \frac{\pi}{4}\left[A(\omega - \Omega_L) + A(\omega + \Omega_L) \right] , \tag{9b}$$

$$(\delta s_{y_1}\delta s_{x_1})_\omega = (\delta s_{x_1}\delta s_{y_1})_\omega^* = \frac{2\mathrm{i}\omega\Omega_L\tau_s^2}{1+\tau_s^2(\omega^2+\Omega_L^2)}(\delta s_{x_1}^2)_\omega , \tag{9c}$$

where a broadened δ-function is introduced in accordance with

$$A(x) = \frac{1}{\pi}\,\frac{\tau_s}{1+(x\tau_s)^2} . \tag{10}$$

It follows from Eqns (9) that the fluctuation of the longitudinal to the magnetic field spin component is unaffected by

the field (the **B**-dependence can arise from the field dependence of the spin relaxation time $\tau_s(B)$). The spin fluctuations transverse to the field precess at the frequency Ω_L, resulting both in a shift of the arguments of the broadened δ-functions in $(\delta s_{x_1}^2)_\omega$, $(\delta s_{y_1}^2)_\omega$ and in the appearance of cross-correlators $(\delta s_{y_1}\delta s_{x_1})_\omega = (\delta s_{x_1}\delta s_{y_1})_\omega^*$.

The Langevin random forces method is not the only one for calculating spin correlators. In many cases, it is convenient to write and solve kinetic equations for the correlation functions $\mathcal{C}_{\alpha\beta}(\tau)$ [31]. In the simplest case under consideration, these equations have the form (at $\tau > 0$)

$$\frac{\partial}{\partial\tau}\,\mathcal{C}_{\alpha\beta}(\tau) + \sum_{\gamma\delta}\epsilon_{\alpha\gamma\delta}\mathcal{C}_{\gamma\beta}(\tau)\,\Omega_\delta + \frac{\mathcal{C}_{\alpha\beta}(\tau)}{\tau_s} = 0\,, \tag{11}$$

where $\epsilon_{\alpha\gamma\delta}$ is the Levi-Civita symbol. In agreement with the general approach, Eqns (11) are supplemented by initial condition (6), which describes single-time correlators. This approach turns out to be particularly convenient for describing spin noise in nonequilibrium conditions [32, 33].

As we already mentioned, the spin correlation functions $\tilde{\mathcal{C}}_{\alpha\beta}(\omega)$ under thermal equilibrium conditions can be expressed via corresponding components of the spin susceptibility. This statement, known as the fluctuation-dissipation theorem, can be formulated as follows. Let us introduce generalized forces **f** with the Cartesian components

$$f_\alpha(t) = f_{\alpha,\omega}\exp(-\mathrm{i}\omega t) + \text{c.c.}\,,$$

which lead to a perturbation of the spin system Hamiltonian in the form

$$\hat{V} = -\sum_\alpha \hat{s}_\alpha f_\alpha\,. \tag{12}$$

We also introduce the spin susceptibility, $\mu_{\alpha\beta}(\omega)$, with respect to these forces in accordance with the linear response theory:

$$\delta s_{\alpha,\omega} = \sum_\beta \mu_{\alpha\beta}(\omega) f_{\beta,\omega}\,. \tag{13}$$

Thus, at high temperatures, $k_B T \gg \hbar\omega$, the spin noise spectrum can be recast as [1, 2]

$$(\delta s_\alpha \delta s_\beta)_\omega = \frac{\mathrm{i}k_B T}{\omega}\left[\mu_{\beta\alpha}^*(\omega) - \mu_{\alpha\beta}(\omega)\right]. \tag{14}$$

This establishes a relation between the spin noise spectroscopy and the electron spin resonance technique. We stress that this relation holds true in thermal equilibrium only. In nonequilibrium systems, the susceptibility to external fields and noise spectra are, generally speaking, independent [29, 30].

Also, spin noise spectra can be expressed via the eigenfunctions and eigenenergies of the spin system [2]; see Section 3 and Eqn (27) therein.

2.2 Onsager relations

Let us now analyze several general properties of correlation functions. By definition, Eqn (4), the second order correlator $\mathcal{C}_{\alpha\beta}(\tau)$ satisfies the permutation relation

$$\mathcal{C}_{\alpha\beta}(\tau) = \mathcal{C}_{\beta\alpha}(-\tau)\,. \tag{15a}$$

In equilibrium, the time reversal symmetry leads to additional relations for the correlation functions [2]. In the absence of magnetic fields, it is of no importance which of the spin components δs_α or δs_β is taken at the earlier or later moment of time in Eqns (3) and (4). Hence, at $\mathbf{\Omega}_L = 0$, we have $\mathcal{C}_{\alpha\beta}(\tau) = \mathcal{C}_{\beta\alpha}(\tau) = \mathcal{C}_{\alpha\beta}(-\tau) = \mathcal{C}_{\beta\alpha}(-\tau)$. In the presence of a magnetic field in addition to Eqn (15a), we obtain

$$\mathcal{C}_{\alpha\beta}(\tau;\mathbf{\Omega}_L) = \mathcal{C}_{\beta\alpha}(\tau;-\mathbf{\Omega}_L)\,, \tag{15b}$$

because the magnetic field changes its sign at a time reversal $t \to -t$: $\mathbf{\Omega}_L \to -\mathbf{\Omega}_L$. Naturally, correlators in the frequency domain have the same properties. Moreover, since the replacement $\omega \to -\omega$ corresponds to a complex conjugation, it follows then that

$$\tilde{\mathcal{C}}_{\alpha\beta}(\omega) = \tilde{\mathcal{C}}_{\beta\alpha}^*(\omega) = \tilde{\mathcal{C}}_{\beta\alpha}(-\omega)\,, \tag{16a}$$

$$\tilde{\mathcal{C}}_{\alpha\beta}(\omega;\mathbf{\Omega}_L) = \tilde{\mathcal{C}}_{\beta\alpha}(\omega;-\mathbf{\Omega}_L)\,. \tag{16b}$$

Equations (15b) and (16b) are known as Onsager relations. They describe the principle of symmetry of kinetic coefficients in thermal equilibrium conditions [2, 34]. Evidently, Eqn (9) satisfies the principle of symmetry of kinetic coefficients (16).

2.3 Relation between spin noise spectroscopy and Raman scattering of light

In optical experiments on spin noise spectroscopy, as discussed above, the spin noise is detected via fluctuations of the Faraday, Kerr, and ellipticity effects. Fluctuations of the sample magnetization result in a modulation of the polarization of the monochromatic wave transmitted through the sample. As a result, the spectrum of the electromagnetic field is enriched. This results in a relation between fluctuations of the Faraday and Kerr rotations, as well as ellipticity, and the spin-flip Raman scattering of light [35].

Let us address these effects in more detail following Ref. [36]. Let the probe beam polarized along the x-axis with frequency ω propagate through a medium along the z-axis. Then, the contribution to the dielectric polarization of the medium caused by the spin fluctuation $\delta S_z(t)$ can be written in the form [1, 36]

$$\delta P_y \propto \frac{\delta S_z(t) E_{0,x}\exp(-\mathrm{i}\omega t)}{\omega_0 - \omega - \mathrm{i}\gamma}\,, \tag{17}$$

where $E_{0,x}$ is the amplitude of the probe beam, and ω_0 and γ are the eigenfrequency and damping of the resonance of the medium used to detect the spin fluctuations. It is assumed that the detuning $|\omega_0 - \omega|$ is small compared to the distances to other resonances. We also assume that the spin fluctuations $\delta S_z(t)$ are 'slow' compared to γ^{-1}. The presence of an orthogonal to the initial polarization component δP_y of the dipole moment results in polarization plane rotation, with the instantaneous fluctuation of the Faraday rotation angle being [cf. Eqn (1)]

$$\delta\theta_F(t) \propto \mathrm{Re}\left\{\delta P_y E_{0,x}^*\right\} \propto \delta S_z(t)\,\frac{\omega - \omega_0}{(\omega-\omega_0)^2 + \gamma^2}\,. \tag{18}$$

In spin noise spectroscopy experiments, the correlator $\langle\delta\theta_F(t)\,\delta\theta_F(t')\rangle$ (or its Fourier transform) is measured. To that end, a field transmitted through the sample is detected using a photodetector, which enables detection of the light intensity and Stokes parameters (see Fig. 2). Next, the signal arrives at a spectrum analyzer, where the Faraday rotation

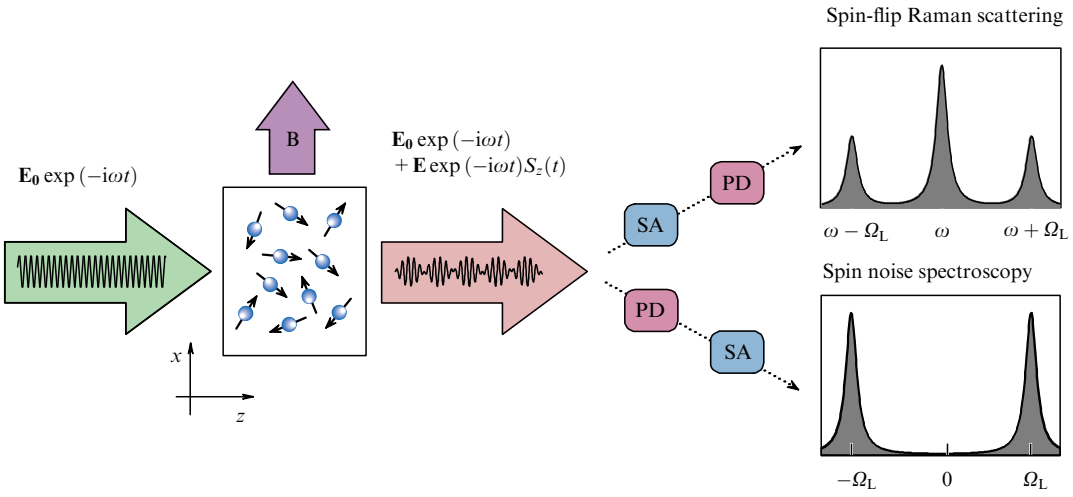

Figure 2. Transmission of the probe beam through a sample. 'SA' denotes the spectrum analyzer and 'PD' denotes the photodetector. In spin-flip Raman scattering experiments, the spectrum analyzer is used in the optical frequency domain. In spin noise spectroscopy, it is used in the radio frequency domain. (Adapted from Ref. [36].)

angle spectrum (generally speaking, the spectrum of light intensity) is acquired [36, 37].

It follows from Eqn (17) that the spectrum of the probe field is enriched due to the fluctuations $\delta S_z(t)$. For example, in the simplest case, when a transverse magnetic field is applied, $\delta S_z(t) \propto \cos(\Omega_L t)$ [cf. Eqn (9b)], spin fluctuations result in the appearance of secondary or scattered waves with the frequencies $\omega \pm \Omega_L$. This secondary field is usually detected in inelastic spin-flip light scattering [35–37], where the field transmitted through the sample is first passed through a spectrometer and then converted into the photocurrent of a detector. As a result, the intensities of corresponding spectral components are detected (Fig. 2). The analysis above underlines the deep connection between the spin noise spectroscopy technique and spin-flip Raman scattering: both methods allow one to determine the correlation function of spin fluctuations.

3. Zero dimensional systems

Semiconductor systems with localized charge carriers are among the most studied using the spin noise spectroscopy technique. The key attractive feature of such systems is a long — up to micro- or even milliseconds — spin relaxation time in typical samples with quantum dots, which results from quenching of spin relaxation mechanisms related to the orbital motion of electrons. The main cause of the spin decoherence of localized charge carriers is, as a rule, the hyperfine interaction with host lattice nuclear spins [1]. In this section, we describe the spin noise spectra in systems with pronounced hyperfine interaction in moderate magnetic fields.

3.1 Central spin model

The spin Hamiltonian of a localized electron in an external magnetic field **B** in the presence of a hyperfine interaction with the host lattice nuclear spins has the form

$$\mathcal{H} = \hbar\mathbf{\Omega}_L\mathbf{S} + \sum_{k=1}^{N_n} A_k\mathbf{I}_k\mathbf{S}\,. \tag{19}$$

Here, **S** is the electron spin operator, $\mathbf{\Omega}_L = g_e\mu_B\mathbf{B}/\hbar$ is the Larmor precession frequency in an external magnetic field, g_e is the effective electron g-factor (its anisotropy is disregarded), subscript k enumerates N_n nuclear spins which efficiently interact with the electron spin, $\mathbf{I}_k$ are the nuclear spin operators, and A_k are the hyperfine coupling constants. The latter are determined both by the parameters of isotopes of the lattice and by the electron wavefunction [1, 38]. The magnetic field, as before, is assumed to be quite weak, and the temperature is assumed to be sufficiently large to ignore the average electron spin polarization. In thermal equilibrium, the nuclear spins are oriented randomly; therefore, the electron experiences a random nuclear field

$$\hbar\mathbf{\Omega}_N = \sum_{k=1}^{N_n} A_k\mathbf{I}_k\,. \tag{20}$$

In real III–V semiconductor systems, the number of nuclei in a quantum dot is $N_n \sim 10^4$–10^6. The mean square fluctuation of the nuclear field is given by $\langle\mathbf{\Omega}_N^2\rangle = 3\delta_e^2/2$, where the parameter δ_e is defined as

$$\delta_e^2 = \frac{2}{3}\sum_{k=1}^{N_n} I_k(I_k+1)\frac{A_k^2}{\hbar^2}\,. \tag{21}$$

The description of the intertwined spin dynamics of electron and nuclei in the framework of Hamiltonian (19) is known in the literature as the central spin model [39, 40].

In the framework of the model described by Eqn (19), the nuclear spin dynamics are driven by the electron spin. Generally, the nuclear spin dynamics in quantum dots can also be related to the quadrupole interaction, i.e, the splitting of nuclear spin levels due to strain and nuclear spin precession in the external magnetic field. Corresponding characteristic times exceed by far the electron spin precession period in the field of nuclear fluctuation $\sim 1/\delta_e$. This is because of the small nuclear g-factor and quadrupole splittings, as well as the small ratio of the Knight and Overhauser fields of the order of $1/\sqrt{N_n}$. Due to the separation of the timescales, nuclear spins at times relevant for the electron spin dynamics can be considered frozen [41]. In this case, one can apply a 'semiclassical' approach to describe the spin noise [30], which is based on the averaging of the dynamics of the electron spin fluctuations over the distribution of $\mathbf{\Omega}_N$.

Hence, for a given direction of the nuclear field, the electron spin correlation functions are given by Eqn (9), where $\mathbf{\Omega} = \mathbf{\Omega}_\mathrm{L} + \mathbf{\Omega}_\mathrm{N}$ is the total electron spin precession frequency. Due to the large number of nuclei, $N_\mathrm{n} \gg 1$, and the statistical independence of their spins, the distribution function of nuclear fields is Gaussian [41]:

$$\mathcal{F}(\mathbf{\Omega}_\mathrm{N}) = \frac{1}{(\sqrt{\pi}\delta_\mathrm{e})^3} \exp\left(-\frac{\Omega_\mathrm{N}^2}{\delta_\mathrm{e}^2}\right). \tag{22}$$

In the case of holes, the hyperfine interaction is anisotropic, so the dispersions of the Overhauser field as well as the effective g-factors in different directions can differ [42, 43]. Making use of Eqn (9), one can readily calculate the spin noise spectrum per electron [30],

$$(\delta S_z^2)_\omega = \frac{\pi}{2}\int \mathrm{d}\mathbf{\Omega}_\mathrm{N}\, \mathcal{F}(\mathbf{\Omega}_\mathrm{N}) \times \left\{\cos^2\theta\, \Delta(\omega) + \sin^2\theta\, \frac{\Delta(\omega-\Omega)+\Delta(\omega+\Omega)}{2}\right\}, \tag{23}$$

where θ is the angle between $\mathbf{\Omega}$ and the z-axis and τ_s in $\Delta(x)$ [see Eqn (10)] is the phenomenological spin relaxation time unrelated to the hyperfine interaction. In the 'box' model, where all hyperfine coupling constants are equal, the number of nuclear spins is large, and an external field is absent, Eqn (23) is exact [44, 45]. The case of a nonzero field is analyzed in [46].

As a rule, the spin relaxation time is much longer than the spin precession period in the nuclear field, i.e, the condition $\delta_\mathrm{e}\tau_\mathrm{s} \gg 1$ holds. In this case, it is possible to derive an analytical expression for the spin noise spectrum in a zero magnetic field:

$$(\delta S_z^2)_\omega = \frac{\pi}{6}\Delta(\omega) + \frac{2\sqrt{\pi}\omega^2}{3\delta_\mathrm{e}^3}\exp\left(-\frac{\omega^2}{\delta_\mathrm{e}^2}\right), \tag{24}$$

which is shown by the black curve *1* in Fig. 3. The spectrum consists of two peaks. The first one at the zero frequency, is very high and narrow. It corresponds to relaxation with time constant τ_s of the spin component parallel to $\mathbf{\Omega}_\mathrm{N}$. This peak is denoted as relaxational. The second peak, with the maximum at $\omega = \delta_\mathrm{e}$, corresponds to the electron spin precession in a random nuclear field, its shape reflects the distribution function of the absolute value $\mathbf{\Omega}_\mathrm{N}$, and its width is of the order of δ_e.

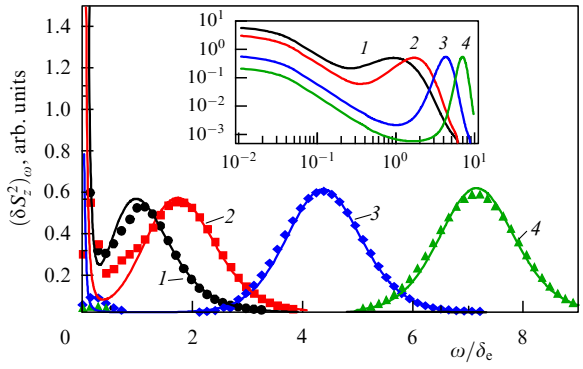

Figure 3. (Color online.) Spin noise spectra calculated according to Eqn (23) (solid curves) and numerically in the central spin model taking into account the nuclear spin dynamics (dots) for different transverse external fields $\Omega_\mathrm{L} = 0$ (black *1*), $\Omega_\mathrm{L} = \sqrt{2}\delta_\mathrm{e}$ (red *2*), $\Omega_\mathrm{L} = 3\sqrt{2}\delta_\mathrm{e}$ (blue *3*), $\Omega_\mathrm{L} = 5\sqrt{2}\delta_\mathrm{e}$ (green *4*) for $\tau_\mathrm{s}\delta_\mathrm{e} = 25\sqrt{2}$. Inset shows solid curves in the bilogarithmic scale.

Note that the spectral weight of the zero frequency peak is 1/3 of the total intensity of the spin noise. This is a result of the isotropic distribution of hyperfine fields. Application of the transverse external magnetic field reduces the probability of finding the total field $\mathbf{\Omega}$ parallel to the z-axis. This probability is proportional to $\cos^2\theta$. As a result, the peak at the zero frequency gets suppressed, while the precession peak shifts to the higher frequencies, as shown in Fig. 3. In the high-field limit, $\Omega_\mathrm{L} \gg \delta_\mathrm{e}$, the spin noise spectrum has the form

$$(\delta S_z^2)_\omega = \frac{\sqrt{\pi}}{4\delta_\mathrm{e}}\exp\left(-\frac{(\omega-\Omega_\mathrm{L})^2}{\delta_\mathrm{e}^2}\right). \tag{25}$$

It follows from Eqn (25) that the spectrum is Gaussian, centered at Ω_L, with the width determined by a typical fluctuation of the Overhauser field. For electrons localized in quantum dots, as a rule, the spread of g factors is present, resulting in additional broadening of the spectrum, which linearly increases with an increase in the field [12].

The effect of the longitudinal magnetic field is opposite. It results in a decrease in the typical values of the angle θ in Eqn (23), i.e., in the suppression of the precessional peak and enhancement of the relaxational one. In the strong magnetic field limit, $\Omega_\mathrm{L} \gg \delta_\mathrm{e}$, the spin noise spectrum is Lorentzian,

$$(\delta S_z^2)_\omega = \frac{\pi}{2}\Delta(\omega), \tag{26}$$

and it is centered at $\omega = 0$. Its height is three times larger than in the case of a zero field. In quantum dot ensembles, the shape of the peak differs from Lorentzian, which corresponds to nonmonoexponential spin relaxation in the longitudinal magnetic field [13]. In a single quantum dot, the zero-frequency peak is well described by the Lorentzian function [14].

The model described above was successfully applied to describe the spin noise and determine the spin parameters in quantum dot ensembles doped with electrons and holes [47].

The results presented above were derived in the model where the nuclear spin dynamics is ignored. The central spin model can account for the nuclear spin precession in the Knight field. Generally, the spin noise spectrum can be calculated as

$$(\delta S_z^2)_\omega = \frac{2\pi}{\mathcal{N}}\sum_{n,m}\langle n|S_z|m\rangle\langle m|S_z|n\rangle\,\Delta\left(\omega - \frac{E_n - E_m}{\hbar}\right), \tag{27}$$

where $n, m = 1, \ldots, \mathcal{N}$ enumerate eigenstates of Hamiltonian (19), and E_n and E_m are their energies.

Despite the fact that the central spin model can be exactly solved by the Bethe ansatz [39], the actual calculations are most efficiently performed in the time representation by decomposition of the evolution operator $\exp(-i\mathcal{H}\tau/\hbar)$ over the Chebyshev polynomials [48]. This ensures a uniform convergence, regardless of the initial state of the system. Since the number of eigenstates $\mathcal{N}$ exponentially increases with an increase in the number of nuclei N_n, in actual calculations it is possible to address only several tens of nuclei (apart from the case of the simplified 'box' model [44, 45]). An advantage of the numerical approach is the possibility of exactly taking into account the quadrupole splitting of nuclear spin sublevels [49].

The results of numerical calculations [50] are shown by dots in Fig. 3. It is seen that the shape of the precessional peak almost coincides in both approaches. The agreement becomes better with an increase in the number of nuclear spins in the numerical modeling. The agreement is almost complete at the transverse magnetic field $\Omega_L \gtrsim \delta_e$.

From an experimental point of view, peak broadening due to the hyperfine interaction and g-factor distribution can be considered to have a detrimental effect on applications. In Refs [51, 52], an application of an alternating magnetic field to overcome it has been suggested. It results in a series of narrow peaks with a width of $1/\tau_s$ at frequencies determined by the field modulation frequency. If, in addition to the alternating field, the system is subject to a static magnetic field, the spin noise spectra demonstrate the Mollow triplet structure [53]. It can be used to measure the spin relaxation time τ_s under conditions when it is long compared to the spin dephasing time $T_2^* \sim 1/\delta_e$. This kind of experiment has been performed for potassium atoms [54], and it is worthwhile to carry out similar studies for quantum dots.

In addition to the problem of calculating the spin noise of an electron interacting with a large number of nuclei, one can analytically describe spin fluctuations of an electron interacting with a single nuclear spin **I**. This situation is realized, for example, for donor-bound electrons in isotopically purified II–VI semiconductors [55, 56]. Since the isotropic hyperfine interaction conserves the total spin, it is convenient to project the Hamiltonian of the system onto a subspace, where the total spin component along the magnetic field axis is $I_{z_1} + S_{z_1} = m + 1/2$. For $m = -I, \ldots, I-1$, this 'shortened' Hamiltonian can be written as (for states with $m = -I-1$ where the spin dynamics of I is absent)

$$\mathcal{H}_m = \hbar(\mathbf{\Omega}_m + \mathbf{\Omega}_L)\,\mathbf{S} - \frac{A}{4}\,, \tag{28}$$

where $\hbar\Omega_m \equiv \hbar\Omega = (I+1/2)A$ is the splitting between the states with the total momenta $I \pm 1/2$ in the absence of a magnetic field, A is the hyperfine coupling constant, and the direction of the vector $\mathbf{\Omega}_m$ is determined by its component $\hbar\Omega_{m,z} = (m+1/2)A$. Here, as above, we ignore Zeeman splitting of nuclear spin sublevels. For a zero magnetic field, after averaging over all values of m, we find the spin correlation function in the following form:

$$\langle S_z(0)S_z(t)\rangle = \frac{\exp(-t/\tau_s)}{12(2I+1)^2} \times \left[4I^2 + 4I + 3 + 8I(I+1)\cos(\Omega t)\right]. \tag{29}$$

The corresponding spin noise spectrum consists of two peaks at $\omega = 0$ and $\omega = \Omega$. For a transverse magnetic field, for $I = 1/2$, the spin correlator has the form

$$\langle S_z(0)S_z(t)\rangle = \frac{\exp(-t/\tau_s)}{4}\cos\left(\frac{\Omega t}{2}\right) \times \left[\cos\left(\frac{\Omega_L t}{2}\right)\cos\left(\frac{\tilde{\Omega} t}{2}\right) - \frac{\Omega_L}{\tilde{\Omega}}\sin\left(\frac{\Omega_L t}{2}\right)\sin\left(\frac{\tilde{\Omega} t}{2}\right)\right], \tag{30}$$

where $\tilde{\Omega} = \sqrt{\Omega_L^2 + (A/\hbar)^2}$. The corresponding spin noise spectrum is shown in Fig. 4. Generally, it consists of four peaks at the frequencies $\omega = |\Omega \pm \Omega_L \pm \tilde{\Omega}|/2$. In the strong field limit $\Omega_L \gg \Omega$, the spectrum consists of two peaks at

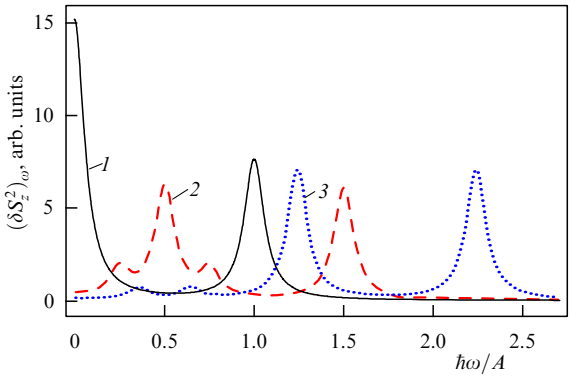

Figure 4. Spin noise spectrum of an electron interacting with donor spin $I = 1/2$ in external magnetic fields $\hbar\Omega_L/A = 0$ (solid black curve *1*), 0.75 (dotted red curve *2*), and 1.6 (dotted blue curve *3*), calculated from correlation function Eqn (30).

$\Omega_L \pm \Omega/2$ [46, 57]. A weak magnetic field shifts the relaxational peak towards the frequency $\Omega_L/2$, which corresponds to an effective g-factor of $g_e/2$. Indeed, a weak field does not mix the singlet and triplet states of the electron-nucleus system; thus, the total spin precesses at half the frequency of the electron. In the general case of $I > 1/2$, the small-field effective g-factor equals $g_e/(2I+1)$ [58].

3.2 Effect of exchange interaction

Many-body effects can be prominent in ensembles of localized electrons. Let us consider, for example, an ensemble of donor-bound electrons in a bulk GaAs-type semiconductor. A typical magnitude of the electron spin precession frequency is $\delta_e \sim 2 \times 10^8$ s^{-1} [10, 59]. Electron–electron exchange interaction becomes comparable to the hyperfine interaction at distances between the donors of about 0.1 μm, which corresponds to the donor density $n_d = 10^{14} - 10^{15}$ cm^{-3}. Since in GaAs the metal-insulator transition takes place at much higher donor densities $\sim 2 \times 10^{16}$ cm^{-3} [60], one has to take into account an interplay between the electron–electron exchange interaction and hyperfine interaction between electron and nuclear spins to describe the spin noise of donor-bound electrons in a bulk semiconductor even at a relatively low doping level. This interplay from the point of view of spin noise has been theoretically studied in Ref. [61].

A model of clusters has been proposed, where the ensemble of donors is divided into groups where the exchange interaction is more efficient then the hyperfine one. Inside the cluster, the spin dynamics is controlled by both the exchange and hyperfine interaction, while the exchange interaction between the clusters can be disregarded. It can be said that a many-body localization of spin excitations on clusters takes place.

Competition between hyperfine and exchange interaction effects can be most simply described, for the illustrating case of two electrons strongly bound by the exchange interaction. Ignoring the hyperfine interaction, the states of the pair of electrons are characterized by the total spin $S = 0$ (singlet) and $S = 1$ (triplet) and spin component S_z along a given axis z. If the splitting between the singlet and triplet is large enough, the mixing of these states via the hyperfine interaction can be disregarded. One can, therefore, consider separately the dynamics of the triplet state with the total spin $S = 1$. Fluctuations $\delta\mathbf{S}$ of the triplet spin state are

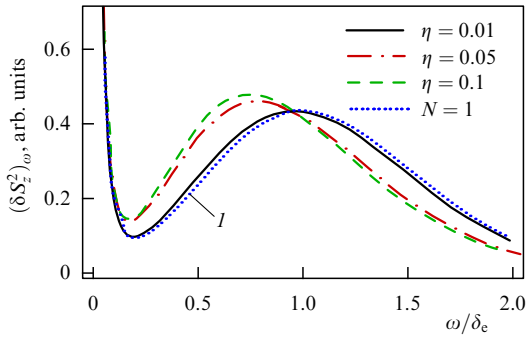

Figure 5. (Color online.) Spin noise spectrum of donor ensembles with different dimensionless densities $\eta = \pi n_d R_c^3/6$. Dotted blue curve was calculated disregarding the exchange interaction. (Adapted from Ref. [61].)

described by Eqn (5) with the effective nuclear field

$$\mathbf{\Omega}_{\text{eff}} = \frac{\mathbf{\Omega}_1 + \mathbf{\Omega}_2}{2}\,. \tag{31}$$

The dispersion of $\mathbf{\Omega}_{\text{eff}}$ is half that of the nuclear fields $\mathbf{\Omega}_1$ and $\mathbf{\Omega}_2$ acting on two electrons. Hence, the spin noise spectrum normalized per electron is given by Eqn (24) with the replacement of δ_e by $\delta_e/\sqrt{2}$. As a result, the peak at $\omega = 0$ is the same as in the absence of the exchange interaction, while the peak resulting from spin precession is shifted to the frequency $\delta_e/\sqrt{2}$, its height increases by a factor of $\sqrt{2}$, and its width, respectively, decreases by a factor of $\sqrt{2}$ compared with that of the peak in the absence of the exchange interaction. This is due to an effective averaging of the nuclear fields caused by the exchange interaction.

In the ensemble of donors, with an increase in electron density characterized by a dimensionless parameter $\eta = \pi n_d R_c^3/6$, where R_c is the distance between the donors with the exchange interaction equal to $\hbar\delta_e$, the precessional peak in the spin noise spectrum shifts to lower frequencies (see Fig. 5), in qualitative agreement with the experimentally observed increase in spin relaxation time with an increase in the density of the donor-bound electrons in bulk GaAs [60].

At a sufficiently high density of donors, the cluster model described above can not be applied. In this case, an infinite cluster is formed in the system, which corresponds, in the classical description, to percolation, and in the quantum description, to a delocalization of spin excitations by many-body interactions. The spin diffusion takes place over the infinite cluster, which, due to hyperfine fields, results in spin relaxation [62]. The spin noise spectrum in this situation consists of a single zero-frequency peak with the width controlled by the spin relaxation time. Modification of the spin noise spectra with an increase in the donor density is discussed in more detail below in Section 3.4.

3.3 Effect of electron hopping

Apart from the exchange interaction, electron hopping between the localization sites can also result in quantitative and even qualitative modification of the spin noise spectra. When only a small fraction of localization centers is occupied with electrons, the spin noise spectrum can be found from single-particle kinetic equations:

$$\frac{d\mathbf{S}_i}{dt} = \mathbf{\Omega}_i \times \mathbf{S}_i + \sum_j (W_{ij}\mathbf{S}_j - W_{ji}\mathbf{S}_i) - \frac{\mathbf{S}_i}{\tau_s}\,, \tag{32}$$

where $\mathbf{S}_i$ is the average spin at the ith site, $\mathbf{\Omega}_i$ is the corresponding precession frequency in a field of the nuclei, and W_{ij} are the hopping rates between the centers. According to a general rule, the correlation functions $\langle \delta S_{i,\alpha}(t+\tau)\, \delta S_{j,\beta}(t)\rangle$ satisfy the same set of equations [3], which should be solved together with initial conditions describing the same-time correlators (see Section 2). This set of equations can be solved analytically provided that the rates of all transitions are equal to each other: $W_{ij} = W_0/N$, where W_0 is the rate of electron departure from a given site, and N is the total number of sites. The spectrum of the total spin fluctuations per electron, $\mathbf{S} = \sum_i \mathbf{S}_i$, in this model has the form [64]

$$(\delta S_z^2)_\omega = \frac{\tau_\omega}{4}\,\frac{\mathcal{A}(\tau_\omega)}{1 - W_0\tau_\omega\mathcal{A}(\tau_\omega)} + \text{c.c.}\,, \tag{33}$$

where $1/\tau_\omega = 1/\tau_s + W_0 - i\omega$ and

$$\mathcal{A}(\tau) = \left\langle \frac{1 + \Omega_{i,z}^2\tau^2}{1 + \Omega_i^2\tau^2} \right\rangle, \tag{34}$$

with the averaging performed over all sites. This expression is valid both in the absence of an external field and when the field is applied along the z-axis. Expressions for the spin noise in the transverse field are more cumbersome; they are given in Ref. [64].

When the field is absent, averaging with distribution function (22) can be done analytically with the result

$$\mathcal{A}(\tau) = \frac{1}{3} + \frac{4}{3(\delta_e\tau)^2} - \frac{4\sqrt{\pi}\exp\left(1/(\delta_e\tau)^2\right)}{3(\delta_e\tau)^3}\,\text{erfc}\left(\frac{1}{\delta_e\tau}\right). \tag{35}$$

Depending on the ratio W_0/δ_e, the shape of the spectrum can be qualitatively different, as will be discussed in more detail in Section 3.4. This model well describes the Si donor bound electron spin noise in GaAs [65] and the Al donor bound electron spin noise in CdTe [63], as illustrated in Fig. 6.

The model with $N \gg 1$ described above neglects the effects of electron return to the initial localization center. These effects can be easily described for a pair of localized electrons [66]. Spin noise spectra for two electrons taking into account the exchange and hyperfine interactions, as well as electron hopping between sites, have a universal low-frequency divergence $\sim \ln(1/\omega)$. It is caused by competition between the spin blockade effect [67, 68] and nuclei-induced electron spin precession. Indeed, if for two electrons the frequencies of spin precession are parallel, $\mathbf{\Omega}_1 \parallel \mathbf{\Omega}_2$, then, in the triplet state, where the electron spins are parallel to the axis of frequencies, electron hops are forbidden, and the spin relaxation (at $\tau_s \to \infty$) is absent. If the angle between the hyperfine fields θ is small, the spin fluctuations decay due to electron hopping between the sites as [69]

$$\delta\mathbf{S}(t) \propto \exp\left(-\frac{\gamma[1 - \cos(\theta)]\,t}{2}\right), \tag{36}$$

where γ is the hopping rate in the singlet state. Averaging of this expression over the directions of nuclear fields results in long-time asymptotic behavior $\propto 1/t$, which corresponds to the logarithmic divergence of the spectra at low frequencies. For a small number N of interacting electrons, the same arguments demonstrate that the spin fluctuations decay as $1/t^{N-1}$; thus, the noise amplitude at low frequencies remains

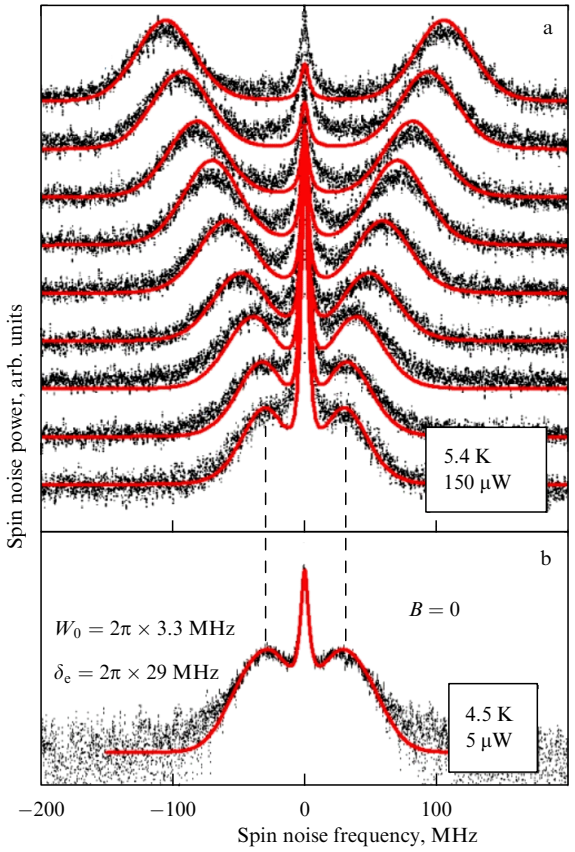

Figure 6. (Color online.) Spin noise spectra in n-doped CdTe (a) in a field from 0 to 4 mT with steps of 0.5 mT (spectra are offset vertically for clarity), (b) in a zero magnetic field. Red curves demonstrate the fit using the model of Eqn (32). (Adapted from Ref. [63].)

finite even at $\tau_s \to \infty$. Hence, the effects of electron returns result, generally speaking, in qualitative modification of the spin noise spectra at low frequencies. Note that there is an exponentially wide spread of the transition rates W_{ij} in real systems, which may result in additional features of low-frequency spin fluctuations [69].

3.4 Effect of quantum-mechanical tunneling

The spin noise spectra can be modified by the electron tunneling between the localization centers apart from the effects of exchange interaction and hopping. In this section, we assume, for simplicity, that the electron density is much lower than the density of the localization sites. Thus, we disregard the electron-electron interaction. We also assume that inelastic hopping is absent, e.g., due to the low temperature. In this situation, the system Hamiltonian has the form

$$\mathcal{H} = \sum_{i,\,j,\,\sigma} t_{ij} c^{\dagger}_{i,\sigma} c_{j,\sigma} + \hbar \sum_i \mathbf{\Omega}_i \mathbf{S}_i \,, \tag{37}$$

where t_{ij} are the tunneling matrix elements between the centers, and $c_{i,\sigma}$ is the annihilation operator of the electron in the spin state σ at the site i. The spin noise spectrum in this case can be calculated using Eqn (27).

It is instructive to compare the modifications of the noise spectra in the models described above, which account for an exchange interaction, electron hopping, and tunneling. With this in mind, we have calculated the spin noise spectra for an ensemble of $N = 10$ randomly and independently distributed sites with different densities using the periodic boundary conditions. For the three models under consideration, we have chosen the analogous set of parameters: (a) exchange interaction constants $J_{ij} = J_0 \exp(-r_{ij}/a_B)$, (b) hopping rates $W_{ij} = W_0 \exp(-r_{ij}/a_B)$, and (c) tunneling constants $t_{ij} = t_0 \exp(-r_{ij}/a_B)$, with $J_0/(\hbar\delta) = W_0/\delta = t_0/(\hbar\delta) \gg 1$, where a_B is the Bohr radius. The results of the calculations are presented in Fig. 7.

Since the characteristic distance between the centers is $l = n^{-1/3}$, the shape of the spectra is determined by a dimensionless parameter $\xi = J_0 \exp(-l/a_B)/(\hbar\delta) = W_0 \exp(-l/a_B)/\delta = t_0 \exp(-l/a_B)/(\hbar\delta)$. For the black curves in Fig. 7, this parameter is small ($\xi \sim 10^{-17}$). In this case, the hyperfine interaction of electron and nuclear spins is much stronger than the coupling with the other centers. The spin noise spectrum is, therefore, described by Eqn (24). With an increase in the density, the spin gets distributed over several centers. In the case of the exchange interaction (Fig. 7a), as described in Section 3.2, a many-body localization on small clusters takes place [70, 71], and afterwards the spin becomes distributed over all N sites. In this case, the nuclear fields are effectively averaged, so the spin precession peak shifts to lower frequencies. As noted above, the spin noise spectrum consists of a single peak at zero frequency in the limit of an infinite number of localization sites and their high density.

In the case of hopping, the spin fluctuations are also delocalized. Qualitatively, the electron spin precesses in the effective magnetic field, which changes with time as a result of electron hopping between the centers with different $\mathbf{\Omega}_{N,i}$. If the hops are inefficient, $W_0/\delta_e \ll 1$, they only broaden the zero frequency peak. In this case, Eqn (24) holds with the

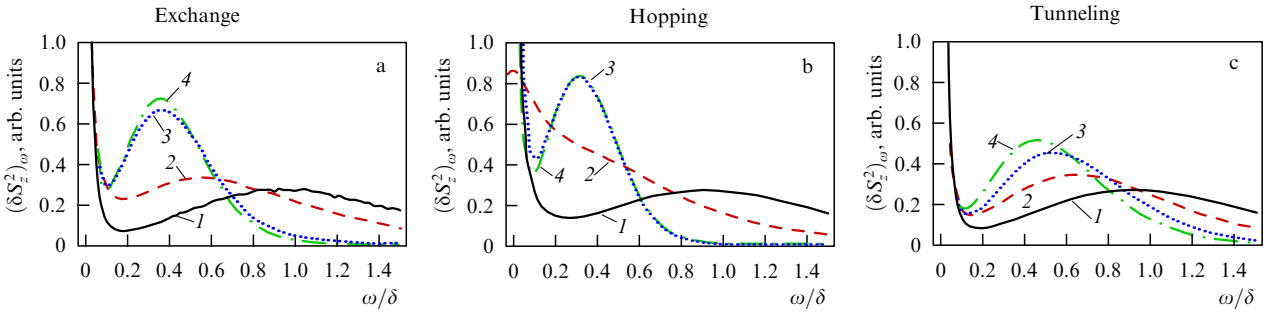

Figure 7. (Color online.) Spin noise spectra of localized electrons calculated taking into account (a) the exchange interaction (Section 3.2), (b) hopping (Section 3.3), and (c) quantum-mechanical tunneling (Section 3.4). Parameters of calculations are $J_0/(\hbar\delta) = W_0/\delta = t_0/(\hbar\delta) = 10^3$ and $\tau_s\delta = 100$, density of centers $na_B^3 = 10^{-4}$ (black *1*), 10^{-3} (red *2*), 10^{-2} (blue *3*), and 10^{-1} (green *4*).

replacement $\tau_s^{-1} \to \tau_s^{-1} + 2W_0/3$. At a higher density of centers and higher temperature, when the hopping becomes fast, $W_0/\delta_e \gg 1$, a dynamical averaging of nuclear fields takes place. In the infinite system, $N \to \infty$, the spin noise spectrum has a Lorentzian shape with the width $\sim \delta_e^2/W_0$. Note that, for the green curve in Fig. 7b, the electron travel time around all N centers is shorter than the spin precession period; thus, the fields of all the centers are averaged.

The case of quantum-mechanical tunneling is qualitatively different from those described above. This is because, even if the parameter ξ is not small, the electrons are localized by the Lifshitz mechanism [72, 73]. The origin is the exponentially broad distribution of the tunneling constants (strong 'off-diagonal' disorder). With an increase in density, the localization length slowly increases, and the spin precession peak shifts to lower frequencies. However, in contrast to the previous cases, the electron delocalization takes place at much higher densities, when $na_B^3 \sim 1$. This regime is not reached for the parameters of the calculations used for Fig. 7.

Interestingly, in the model where the nuclear fields are absent, but the exchange interaction between the localized electrons is present with an exponentially broad distribution of the coupling constants, the many-body localization of the spin fluctuations due to this spread (i.e., by a mechanism analogous to the Lifshitz model) does not take place. The localization is prevented by the conservation of the total angular momentum. It is clear, for example, that the state with the maximal total spin of all electrons is many-body delocalized [74]. An analysis of the symmetries of the Hamiltonian shows that the system in this case is ergodic [70]. If the total angular momentum conservation law is broken, e.g., in the case of anisotropic exchange interaction, the system allows a many-body localization. Such situations are analyzed in more detail in the next Section 4 in respect to the fluctuations in one-dimensional spin chains.

3.5 Spin noise in nonequilibrium conditions

Initially, spin noise spectroscopy was considered a tool to study the spin properties of a system under conditions close to thermal equilibrium [11, 13]. Indeed, the fluctuation dissipation theorem is applicable in this case, and the spin noise spectrum reflects the frequency dependence of the imaginary part of the spin susceptibility (see Eqn (14)). If the system is brought out of equilibrium, e.g., in conditions of the optical orientation of spins, the fluctuation dissipation theorem is not applicable. This situation requires development of the corresponding microscopic theory of nonequilibrium spin noise analogous to that of nonequilibrium fluctuations of electric current [27, 29, 33, 75, 76]. In this case, spin noise spectroscopy allows one to obtain more information about the system dynamics than in the equilibrium conditions [54]. For bulk semiconductors under optical orientation conditions, this problem was solved in the pioneering study [77].

As we have already demonstrated, the spin dynamics of localized charge carriers are mainly controlled by hyperfine interaction with the host lattice nuclei. Naturally, a question arises about the modification of the spin noise spectra when the nuclear spin system is out of thermodynamic equilibrium. The simplest example is nonequilibrium nuclear spin polarization. Experimentally, it can be achieved using the dynamic polarization of nuclei by circularly polarized light, which will be analyzed in more detail in Section 7. Here, we only note that a considerable (exceeding 50%) nuclear spin polarization suppresses the nuclear spin fluctuations and modifies the

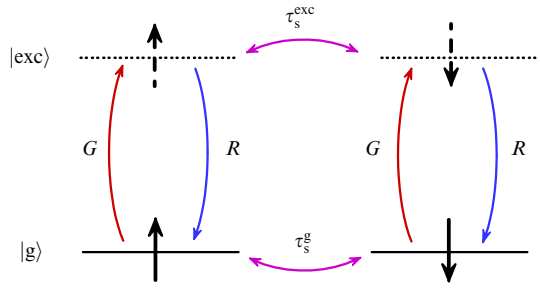

Figure 8. Transitions between ground, $|g\rangle$, and excited, $|exc\rangle$, states of the localization center and of spin relaxation in both states. Solid and dashed thick arrows denote spin component, $S_z^{g,exc}$, in ground and excited states, respectively. (Adapted from Ref. [84].)

distribution function of nuclear spins $\mathcal{F}(\mathbf{\Omega}_N)$ (22) [78]. As a result, the precessional peak in the electron spin noise spectrum can narrow compared with the result of Eqn (25) [79]. Its width can be reduced by several orders of magnitude if the nuclear spin polarization approaches 100%.

The electron spin precession mode-locking effect in the external magnetic field arising in the optical orientation by a train of circularly polarized pulses [80, 81] can serve as another example. The nuclear spins get tuned in such a way that the electron spin precession becomes commensurable with the pulse repetition rate. As a result, the electron spin noise spectrum takes the shape of a sequence of narrow peaks at frequencies satisfying this synchronization condition [82]. Such a structure of the spin noise spectrum directly reveals the nonequilibrium nuclear field distribution function.

Experimentally, the most natural nonequilibrium situation arises when either the absorption of the probe beam or additional nonresonant excitation of the system creates nonequilibrium electrons and holes in a quantum dot. It affects both the dynamics of the system and microscopic mechanisms of the Faraday and Kerr rotation effects. A broad range of nonequilibrium spin noise spectroscopy experiments can be described within the four-level model formulated in Refs [33] and [83]. In this model, in addition to the spin-degenerate ground state, a two-fold degenerate excited state, e.g., the trion state, is taken into account (see Fig. 8).

Let us assume that the excitation and recombination processes in the four-level model conserve the spin z component. The rates of these processes G and R, respectively, do not depend on the spin orientation, as shown in Fig. 8. Thus, the occupancy of the ground state n_g satisfies the equation

$$\frac{dn_g}{dt} = -Gn_g + Rn_{exc}\,, \tag{38}$$

where $n_{exc} = 1 - n_g$ is the occupancy of the excited state. In the steady state,

$$n_g = \frac{R}{R+G}\,. \tag{39}$$

Equations of motion for a spin in the ground state, $\mathbf{S}^g$, and excited state, $\mathbf{S}^{exc}$, have the form

$$\frac{d\mathbf{S}^g}{dt} = \mathbf{\Omega}_g \times \mathbf{S}^g - \frac{\mathbf{S}^g}{\tau_s^g} - G\mathbf{S}^g + G\mathbf{S}^{exc} + \frac{1}{\tau_0} S_z^{exc}\mathbf{e}_z\,, \tag{40a}$$

$$\frac{d\mathbf{S}^{exc}}{dt} = \mathbf{\Omega}_{exc} \times \mathbf{S}^{exc} - \frac{\mathbf{S}^{exc}}{\tau_s^{exc}} - R\mathbf{S}^{exc} + G\mathbf{S}^g\,, \tag{40b}$$

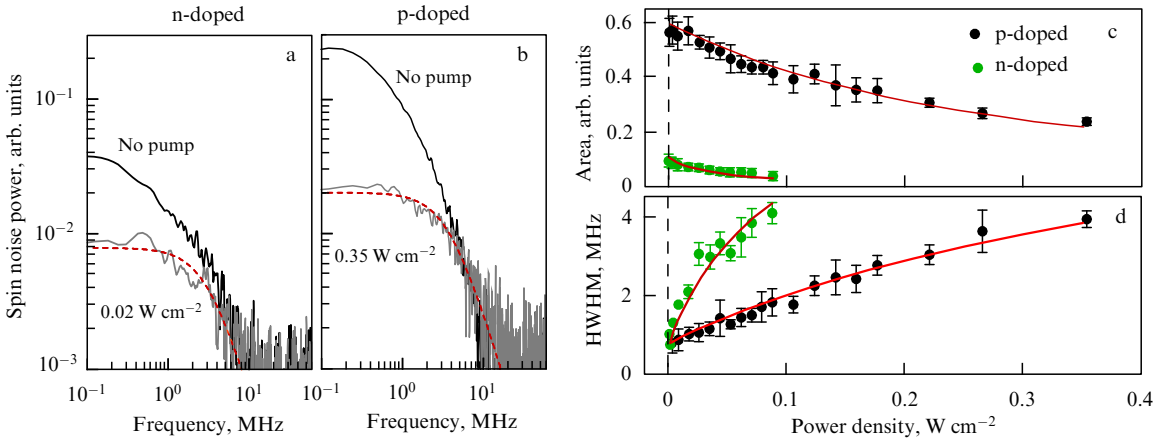

Figure 9. (Color online.) Spin noise spectra in the absence and presence of additional excitation, as indicated in the figure, measured for the samples containing (a) n-type and (b) p-type quantum dots. Red curves show Lorentzian fits. (c) Area under spin noise spectrum as a function of excitation power density for n-type (green dots) and p-type (black dots) sample. (d) Analogous dependence of half-width at half-maximum. (Adapted from Ref. [84].)

where $\mathbf{\Omega}_{\mathrm{g,exc}}$ are the frequencies of the spin precession in the ground and excited states due to both the external magnetic field and hyperfine interaction, $\tau_{\mathrm{s}}^{\mathrm{g,exc}}$ are the phenomenological spin relaxation times, and $\mathbf{e}_z$ is a unit vector along the growth axis of the structure. We have taken into account in Eqns (40) that the rate of recombination (accounting for two-level system saturation effects) can be recast as $R = G + 1/\tau_0$, where τ_0 is the spontaneous trion recombination time. In the latter process, according to the selection rules, only the z-spin component is conserved [33, 85]. Spin noise spectra can be calculated analytically in this model solving the kinetic equations for the spin correlators (see Section 2).

The situation of a nonresonant excitation of singly charged (by electrons or holes) quantum dots is the most illustrative one [84]. Corresponding spin noise spectra are shown in Fig. 9a, b. The spin noise spectra have a Lorentzian form, whose area and half-width are shown in Fig. 9c, d as functions of the excitation power density. The precessional peak in these spectra is at higher frequencies and not shown in the figure.

Despite the fact that, under nonresonant excitation there are many excited states instead of two, the model described above can quantitatively describe the spin noise spectra and their modification due to the generation of nonequilibrium electrons and holes. Assuming that the generation and recombination processes are faster than the spin relaxation, one can show that the average rate of the spin relaxation is a weighted sum of the relaxation rates in the ground and excited states:

$$\frac{1}{\tau_{\mathrm{s}}^{*}} = \frac{n_{\mathrm{g}}}{\tau_{\mathrm{s}}^{\mathrm{g}}} + \frac{n_{\mathrm{exc}}}{\tau_{\mathrm{s}}^{\mathrm{exc}}}\,, \tag{41}$$

where the occupancies of the states are given by Eqn (39). The spin noise power is proportional to n_{g}^2. From a fit of the experimental data, the spin relaxation times $\tau_{\mathrm{s}}^{\mathrm{g}} = 200$ ns and $\tau_{\mathrm{s}}^{\mathrm{exc}} = 19$ ns are obtained for both the studied samples.

In order to enhance the spin signals, one can use microcavities which, however, also increase the amplitude of the electromagnetic field acting on the charge carriers [86]. In the weak coupling regime, the model described above can be used to calculate the nonequilibrium spin noise spectra of charge carriers localized in the quantum well width fluctuations taking into account the absorption of the probe beam and excitation of trions [83]. The spin relaxation of resident charge carriers becomes faster and anisotropic with an increase in the excitation power, and at the same time the effective spin precession frequency decreases. The anisotropy is related to the specifics of the selection rules, according to which the excitation of the trion and its consequent radiative recombination erases the spin components perpendicular to the growth axis of the structure, while this process does not affect the longitudinal spin component (see Eqn (40)).

Figure 10 shows the spin noise spectra measured experimentally (a) and calculated theoretically (b) for different intensities of the probe beam. Generally, the spectra consist of two peaks related to the spin relaxation (at the zero frequency) and the spin precession (at a positive frequency). An increase in the power of the beam results in the suppression of the precessional peak and enhancement of the relaxational peak.

Interestingly, a simplified description of the spin dynamics at a high power of the probe beam can be carried out in the terms of the quantum Zeno effect [87–89]. In agreement with general postulates of quantum mechanics, a continuous detection of electron spin should result in the 'freezing' of the spin dynamics due to the quantum back-action [90]. It results in a renormalization of the spin precession frequency in the external transverse magnetic field Ω_{L} as [91, 92, 200]

$$\Omega = \sqrt{\Omega_{\mathrm{L}}^2 - \lambda^2}\,. \tag{42}$$

Here, the phenomenological parameter λ characterizes the 'measurement strength', which is proportional to the power of the probe beam. In the framework of the four-level model, it can be found that

$$\lambda = \frac{G\tau_{\mathrm{s}}^{\mathrm{exc}}}{2(\tau_{\mathrm{s}}^{\mathrm{exc}} + \tau_0)}\,, \tag{43}$$

so both descriptions of nonequilibrium spin fluctuations are equivalent.

In a microcavity with a single quantum dot, a strong light-matter coupling regime can be realized [86]. Electron spin

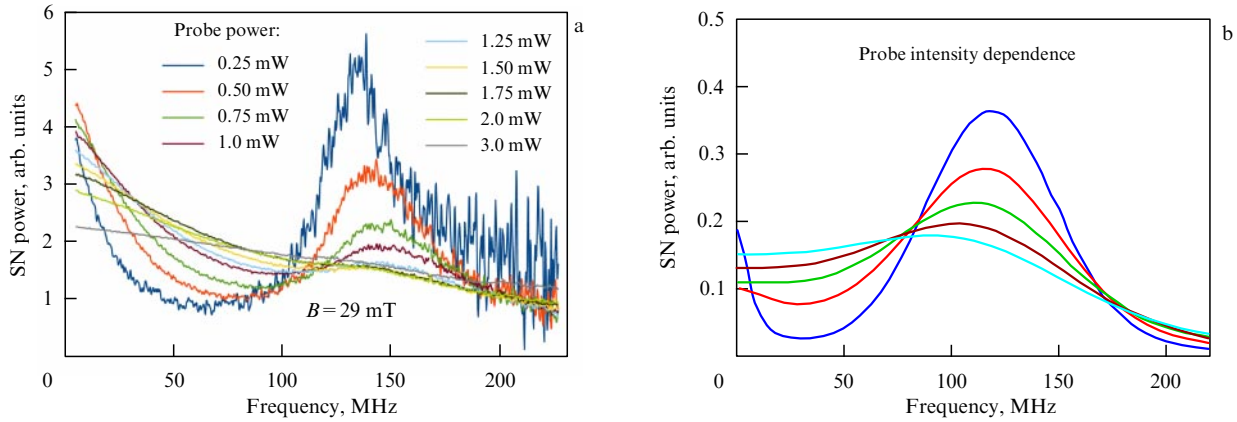

Figure 10. (Color online.) Spin noise spectra under conditions of the generation of singlet trions for different optical excitation powers: (a) experiment, (b) theory. (Adapted from Ref. [83].)

polarization in such structures can result in macroscopic values of the polarization plane rotation angle [93], and it can also allow for a complete reflection of one of the circular components of the probe beam with a complete transmission of the other one. It is important to note that, for a single spin, ensemble averaging does not take place. Therefore, the fluctuations of the optical signals, particularly, those of the reflection and transmission coefficients of light passing through the system, can be macroscopic as well.

A theoretical description of spin noise in the strong-coupling regime requires consideration of the quantum nature of the electromagnetic field. The correlation functions of the Faraday, Kerr, and ellipticity signals can be expressed through the averages of the four field operators in the microcavity, by analogy with the second-order correlation function $g^{(2)}(\tau)$, which describes light intensity fluctuations [94]. These fluctuations depend on the electron spin dynamics due to the fact that, depending on the mutual orientation of the electron spin and photon angular momentum, the light can pass through the cavity or be reflected from it. The simplest optical signal reflecting the spin noise in such a system is the intensity transmission coefficient T of circularly polarized light. Its correlation function, $\langle \delta T(t)\, \delta T(t+\tau)\rangle$, can be expressed as

$$\frac{\langle \delta T(t)\, \delta T(t+\tau)\rangle}{T_0^2} = g^{(2)}(\tau) - 1\,, \tag{44}$$

with T_0 being the average transmission coefficient.

Usually, the spin relaxation time and precession period in an external magnetic field are much longer than the trion recombination time, the photon lifetime in the cavity, and the period of Rabi oscillations between the polariton states. This separation of time-scales allows for developing an analytical approach to calculate the electron and photon dynamics in the system. In the framework of this approach, the expressions for the correlation function of the light transmission coefficients have been derived in the limit of small light intensities [94]. These expressions agree well with numerical calculations based on the density matrix formalism. The spectrum of the transmission coefficient noise, generally, consists of the spin and photon components which contain information, respectively, about the spin dynamics in the system and about the properties of the excited states, such as polariton splitting and the lifetimes of the excited states.

4. Spin chains

Among the most intriguing objects for the analysis of spin dynamics and spin fluctuations are one-dimensional spin chains. Interest in spin diffusion and spin localization in chains is related, on the one hand, to the fact that one-dimensional systems are traditionally used as objects to test theoretical approaches that can also be applied to systems of larger dimensions, and, on the other hand, to the presence of a number of objects that demonstrate pronounced one-dimensional properties [95–98]. Here, we will focus on one of the most studied and widely applied models of spin chains: a spin-1/2 XXZ chain of N sites with disorder described by the Hamiltonian

$$H_{\mathrm{XXZ}} = -J_\perp \sum_{m=1}^{N-1} \left(S_m^x S_{m+1}^x + S_m^y S_{m+1}^y\right) - J_z \sum_{m=1}^{N-1} S_m^z S_{m+1}^z + \hbar \sum_{m=1}^{N} \Omega_m S_m^z\,, \tag{45}$$

where index m numerates N sites in the chain, $J_\perp$ and J_z are the exchange interaction constants between the nearest-neighbor spins, S_m^α are spin components of sites m ($\alpha = x, y, z$), and Ω_m are random magnetic fields at the chain sites oriented along the z-axis. Using a Jordan–Wigner transformation [99], one can map the spin-1/2 XXZ chain model onto a chain of spinless fermions. In this mapping, exchange interaction constants $J_\perp$ and J_z describe fermion hopping between nearest-neighbor sites and nearest-neighbor interaction, respectively, while the terms $\Omega_m S_m^z$ correspond to random on-site energies. In this model, the projection of the total spin $\mathbf{S} = \sum_{m=1}^{N} \mathbf{S}_m$ on the z-axis is conserved.

In particular, for the XX model without disorder, when $J_\perp = J$, $J_z = 0$, and $\Omega_m^z = 0$, the Hamiltonian of the system after Jordan–Wigner transformation has a very simple form,

$$\mathcal{H} = \frac{J}{2} \sum_{m=1}^{N-1} \left(a_m^\dagger a_{m+1} + \mathrm{H.c.}\right), \tag{46}$$

where operators a_m and $a_m^\dagger$ obey the standard commutation rules for fermions and describe annihilation and creation of quasi-particles at the chain sites. The z components of spins are given by

$$S_m^z = a_m^\dagger a_m - 1/2\,, \tag{47}$$

so the problem of spin fluctuations is reduced to the calculation of the correlation function of particle density. Hamiltonian (46) is diagonalized by the Fourier transformation

$$\mathcal{H} = \sum_k E_k a_k^\dagger a_k \,, \tag{48}$$

with the corresponding dispersion law

$$E_k = J\cos k \,, \tag{49}$$

where $a_k = \sqrt{2/(N+1)}\sum_{m=1}^{N} \sin(km)\, a_m$ with $k = \pi n/(N+1)$, and index n takes values $1, 2, 3, \ldots, N$.

Exact expressions for the correlation functions $\langle S_m^z(\tau) S_{m'}^z(0)\rangle$ between the chain sites with indexes m and m' were found for the XX model without disorder [100, 101]. In the limit of an infinite number of sites in the chain, the expression for correlation functions of spin z-components has a simple form:

$$\left\langle S_m^z(\tau) S_{m'}^z(0)\right\rangle = \frac{1}{4} J_{|\Delta m|}^2\left(\frac{J\tau}{\hbar}\right), \tag{50}$$

where the order of the Bessel function $J_{|\Delta m|}(J\tau/\hbar)$ is determined by the absolute value of the difference between chain site numbers $\Delta m = m - m'$ and the argument of the Bessel function depends on the strength of the exchange interaction. Here, as it was done earlier, we assume that the temperature exceeds by far all other energy scales in the system, but the thermalization time is long enough to ignore inelastic processes. The XX model also allows one to obtain exact expressions for the transverse correlation functions $\langle S_m^\alpha(\tau) S_{m'}^\alpha(0)\rangle$, where $\alpha = x, y$, which correspond to the correlations of fermionic operators $a_m^\dagger$, $a_{m'}$ [102–105]. In the case of large number of sites and high temperatures, spin correlation functions for x- and y-components are equal to each other and can be written as

$$\left\langle S_m^x(\tau) S_{m'}^x(0)\right\rangle = \left\langle S_m^y(\tau) S_{m'}^y(0)\right\rangle = \frac{1}{4}\exp\left[-\left(\frac{J\tau}{2\hbar}\right)^2\right]\delta_{m,m'}\,, \tag{51}$$

which corresponds to the spectrum of total spin noise

$$(S_x^2)(\omega) = \frac{N\hbar\sqrt{\pi}}{2J}\exp\left[-\left(\frac{\hbar\omega}{J}\right)^2\right]. \tag{52}$$

These expressions demonstrate that spin fluctuations along the x- and y-axes are localized and do not propagate, while spin fluctuations along the z-axis propagate with the typical velocity $\propto J$ [106, 107], i.e., nondiffusively. It was shown in Ref. [108] that for the XXZ model with $J_z \neq 0$ the behavior of correlation functions changes and can become diffusive.

Let us now analyze spin correlators in the presence of random fields Ω_m, which can be caused, for example, by the hyperfine interaction with the nuclear spins of the crystal lattice. Following Eqn (22), let us consider the Gaussian form of the distribution function of random fields:

$$\mathcal{F}(\Omega) = \frac{1}{\sqrt{\pi}\delta}\exp\left(-\frac{\Omega^2}{\delta^2}\right). \tag{53}$$

For the XX model, any small disorder leads to the localization of spin fluctuations. Formally, this problem is equivalent to the one of noninteracting electron localization in the 1D system with 'diagonal' disorder [109].

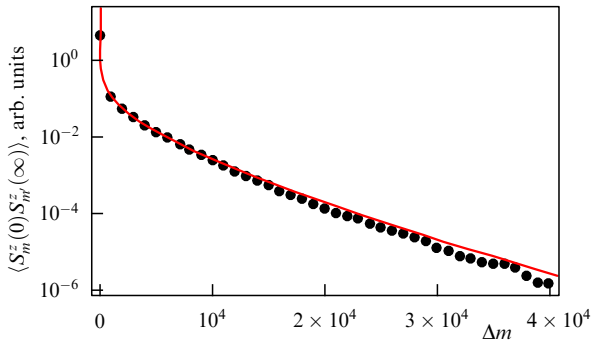

Figure 11. Spin correlation function for the XX model with disorder in the long time limit. Solid curve is calculated analytically; dots correspond to the numerical calculations performed for the 10^5 sites with periodical boundary conditions for $\hbar\delta = 0.035J$.

First, random fields lead to the modification of the density of states, which in the absence of disorder reads

$$\rho_0(E) = \frac{1}{\pi\sqrt{J^2 - E^2}} \tag{54}$$

and diverges in the vicinity of $E = \pm J$, as the velocity of carriers is equal to zero for these energy values (see Eqn (49)). As it was shown in Refs [109, 110], weak disorder ($\delta \ll J$) modifies density of states ρ in the vicinity of the band edges:

$$\rho(E) = \frac{1}{\pi^2}\sqrt{\frac{E_0}{J}}\frac{\mathrm{d}}{\mathrm{d}\Delta E}\frac{1}{\mathrm{Ai}^2(-2\Delta E/E_0) + \mathrm{Bi}^2(-2\Delta E/E_0)}\,, \tag{55}$$

where $\Delta E = \pm E - J$, $E_0 = \hbar\delta\sqrt[3]{\hbar\delta/J}$, and $\mathrm{Ai}(x)$, $\mathrm{Bi}(x)$ are Airy functions of the first and second kind, respectively.

Second, the presence of disorder leads to the localization of wave functions. The distribution function of the inverse localization length $w(A)$ can be found by averaging the distribution function of the inverse localization length for a given velocity over all the wave vectors [111, 112]. The result reads

$$w(A) = \frac{1}{2\pi\mathrm{i}}\int_{-\mathrm{i}\infty}^{\mathrm{i}\infty}\frac{\mathrm{d}x\, x}{A_0\sinh^2(\sqrt{x})} \times \exp\left(\frac{xA}{A_0}\right)\left[I_0\left(\frac{xA}{A_0}\right) + I_1\left(\frac{xA}{A_0}\right)\right], \tag{56}$$

where $A_0 = 3(\hbar\delta)^2/(2J^2)$. Integration is performed along the imaginary axis, $\mathrm{Re}\,(x) = 0$.

Similarly, one can find spin correlation function $\langle S_m^z(0) S_{m'}^z(\infty)\rangle$ in the long time limit, because in this limit one can disregard the interference effects between the wave functions corresponding to the different eigenstates. Figure 11 shows the result of numerical calculations performed for the 10^5 sites. For a fixed value of the particle wave vector $\mathbf{k}$, the localization length is equal to $l_0 = 2J^2/(\hbar\delta)^2\sin^2 k$ [113], and the explicit expression for the correlation function of particle density was found in Ref. [114]. Its long distance asymptotic form is [115]

$$p(\Delta m) \approx \frac{\pi^3\sqrt{\pi}}{16 l_0}\left(\frac{l_0}{\Delta m}\right)^{3/2}\exp\left(-\frac{\Delta m}{l_0}\right). \tag{57}$$

Averaging of the exact correlation function over the wave vectors gives the possibility of obtaining the expression for the spin correlation function in the limit of long distances and high temperature:

$$\left\langle S_m^z(0) S_{m'}^z(\infty)\right\rangle = \frac{\pi^3 J^2}{32\delta^2 \Delta m^2} \exp\left(-\frac{\delta^2}{8J^2}\Delta m\right). \tag{58}$$

For the XXZ model, the localization takes place in the presence of arbitrary small disorder. In this case, the threshold of many-body localization can be studied [116–117]. However, for the isotropic XXX model ($J_\perp = J_z$), the conservation of total angular momentum makes complete many-body localization impossible [70].

The role of inelastic processes in the dynamics of spin correlators in 1D systems is still not well understood. The interplay between electrons hopping between the localized states and hyperfine interaction with nuclear spins of the lattice in a quantum wire was analyzed in Ref. [119]. In the case of a low density of sites, the localization leads to an exponentially broad distribution of the hopping times, resulting in low frequency singularity in the noise spectra. The dynamics of spin fluctuations in this regime can be well described by the model of pairs of closely localized sites and single states, similarly to the model of clusters, which was discussed in the previous Section 3.

5. Two-dimensional systems

The key difference between two-dimensional and one dimensional systems with disorder and zero dimensional systems from the point of view of the spin dynamics and spin noise is the free propagation of the charge carriers. This leads to considerable suppression of the hyperfine interaction, so that the spin dynamics is mainly driven by the spin-orbit interaction.

In structures without an inversion center, the effective Hamiltonian consists of the term responsible for the kinetic energy of a particle $\varepsilon_k = \hbar^2 k^2/2m$, where $\mathbf{k}$ is the quasi-wavevector and m is the effective mass of an electron, and spin-dependent terms, which can be written in the form [15, 120, 121]

$$\mathcal{H}_{\rm so} = \frac{\hbar}{2}(\mathbf{\Omega_k}\boldsymbol{\sigma}). \tag{59}$$

Here, $\mathbf{\Omega_k}$ is the pseudovector with the absolute value and direction strictly related to the electron wavevector $\mathbf{k}$. In quantum well structures based on III–V and II–VI materials and in a number of systems based on silicon and germanium, the components of vector $\mathbf{\Omega_k}$ are linearly related to the components of $\mathbf{k}$. In particular, in quantum wells with the zinc blend structure grown along the $z \parallel [001]$ direction, pseudovector $\mathbf{\Omega_k}$ can be presented in the following form [122–125]:

$$\mathbf{\Omega_k} = (\beta_1 k_y, \beta_2 k_x, 0), \tag{60}$$

where the axes $x \parallel [1\bar{1}0]$ and $y \parallel [110]$ are the main axes of the C_{2v} point symmetry group, which generally characterizes the symmetry of such structures. The constants $\beta_{1,2}$ are determined by the specific structure and microscopic mechanisms of the lifting of the spectrum spin degeneracy. Notably, the case of $\beta_1 = -\beta_2$ corresponds to the dominant structure inversion asymmetry (the Rashba contribution to the spin splitting), and $\beta_1 = \beta_2$ corresponds to the bulk (or in some cases interface) inversion asymmetry (the Dresselhaus contribution).

It follows from the form of effective Hamiltonian (59) that the electron spin precesses in the effective magnetic field with the frequency $\mathbf{\Omega}_k$, which determines the dynamics and relaxation of the spin fluctuations. The regime of the spin dynamics is determined by the relation between the typical frequency Ω_k and the electron collision time τ^* (strictly speaking, the single electron momentum relaxation time, which accounts for the scattering of the static disorder and phonons as well as electron-electron collisions [126, 127]). Hereafter, we assume that the typical spin splitting $\hbar\Omega_k$ is much smaller than the electron kinetic energy, which allows us to ignore the effect of the spin dynamics on the orbital electron motion. In the limit of frequent collisions

$$\Omega_k \tau^* \ll 1, \tag{61a}$$

the relaxation of spin fluctuations is described by the exponential law, and the correlation functions obey the system of equations (cf. Eqn (11) and Refs [2, 124])

$$\frac{\mathrm{d}\mathcal{C}_{\alpha\beta}(\tau)}{\mathrm{d}\tau} + \Gamma_{\alpha\alpha'}\mathcal{C}_{\alpha'\beta}(\tau) = 0,$$
$$\Gamma_{\alpha\beta} = \left\langle (\Omega_{\mathbf{k}}^2 \delta_{\alpha\beta} - \Omega_{\mathbf{k},\alpha}\Omega_{\mathbf{k},\beta})\,\tau^*\right\rangle. \tag{61b}$$

In the tensor of the inverse spin relaxation times $\Gamma_{\alpha\beta}$, the averaging is performed over the electron ensemble described by the equilibrium Fermi–Dirac distribution function $f(\varepsilon_k)$ according to

$$\left\langle F(\mathbf{k})\right\rangle = \frac{\sum_{\mathbf{k}} F(\mathbf{k}) f'(\varepsilon_k)}{\sum_{\mathbf{k}} f'(\varepsilon_k)}.$$

The situation turns out to be fundamentally different when the collisions are relatively rare:

$$\Omega_k \tau^* \gtrsim 1. \tag{62a}$$

In this case, the electron spin rotates by a considerable angle between the consequent collisions, so the spin noise demonstrates an oscillating behavior in time, which is analogous to the spin polarization oscillations after pulsed optical excitation [128–130]. As an example, let us consider equations that describe the dynamics of the correlation function of the z component of the total spin of electron gas for arbitrary $\Omega_k\tau^*$. Let us introduce the auxiliary function

$$C_{zz}(\tau; \mathbf{k}, \mathbf{k}') = \left\langle \left\{ \delta s_{\mathbf{k},z}(t+\tau) \delta s_{\mathbf{k}',z}(t) \right\} \right\rangle,$$

where $s_{\mathbf{k},z}(t)$ is the component of the spin polarization with the wave vector $\mathbf{k}$. We have $\mathcal{C}_{zz}(\tau) = \sum_{\mathbf{k},\mathbf{k}'} C_{zz}(\tau; \mathbf{k}, \mathbf{k}')$. This function obeys the equation

$$\left(\frac{\partial}{\partial\tau} + \frac{1}{\tau^*}\right)\frac{\partial}{\partial\tau} C_{zz}(\tau; \mathbf{k}, \mathbf{k}') + \Omega_k^2 C_{zz}(\tau; \mathbf{k}, \mathbf{k}')$$
$$+ \left(\frac{\partial}{\partial\tau} + \frac{1}{\tau^*}\right)\frac{C_{zz}(\tau; \mathbf{k}, \mathbf{k}') - \bar{C}_{zz}(\tau; \mathbf{k}, \mathbf{k}')}{\tau^*} = 0, \tag{62b}$$

where the bar above the expression denotes averaging over the directions of vector $\mathbf{k}$ for its fixed absolute value. This differential equation of the second order in τ is obtained from equations of the first order for the

correlator $\langle\{\delta s_{\mathbf{k},z}(t+\tau)\,\delta s_{\mathbf{k}',z}(t)\}\rangle$ and the combination $\Omega_{\mathbf{k},y}\langle\{\delta s_{\mathbf{k},x}(t+\tau)\delta s_{\mathbf{k}',z}(t)\}\rangle - \Omega_{\mathbf{k},x}\langle\{\delta s_{\mathbf{k},y}(t+\tau)\delta s_{\mathbf{k}',z}(t)\}\rangle$, accounting for the fact that frequency $\mathbf{\Omega}_\mathbf{k}$ is perpendicular to the z-axis. In particular, for degenerate electrons, isotropic spin splitting in the quantum well plane and $\Omega_{k_\mathrm{F}}\tau^* \gg 1$, where k_F is the Fermi wave vector, we have $C_{zz}(\tau) \propto \cos(\Omega_{k_\mathrm{F}} t)\exp(-t/2\tau^*)$ [128].

Interestingly, the degeneracy of the electron gas leads to the suppression of the spin noise intensity. In can be easily seen from the direct calculation of the equilibrium values of the correlators

$$C_{\alpha\beta}(0) = \frac{\delta_{\alpha\beta}}{4}\sum_\mathbf{k} f(\varepsilon_k)\bigl[1-f(\varepsilon_k)\bigr] \sim \frac{N}{4}\begin{cases}\dfrac{k_\mathrm{B}T}{E_\mathrm{F}}\,, & k_\mathrm{B}T \ll E_\mathrm{F} = \dfrac{\hbar^2 k_\mathrm{F}^2}{2m}\,,\\ 1, & k_\mathrm{B}T \gg E_\mathrm{F}\,.\end{cases} \tag{63}$$

Here, N is the electron concentration. As expected from the qualitative arguments, in the degenerate gas, the electron spins fluctuate only in the states in the energy window $k_\mathrm{B}T$ in the vicinity of the Fermi energy. The filled states with $E_\mathrm{F} - \varepsilon \gg k_\mathrm{B}T$ do not contribute, since in each such state there are two electrons with opposite spins. A similar suppression also takes place in three-dimensional systems with free electrons and was experimentally observed in GaAs crystals [9]. In the finite area, even at zero temperature, the quantum correlations [2] give rise to an additional contribution, which is related to the finite wavelength of the electrons.

The linear relation between the magnetic field $\mathbf{\Omega}_\mathbf{k}$ and the electron wave vector $\mathbf{k}$, as well as the possibility of free electron propagation in the quantum well plane, leads to a number of vivid features of spatio-temporal spin correlators. Let us illustrate these effects by the case of compensation of the Dresselhaus and Rashba terms $\beta_1 \neq 0$, $\beta_2 = 0$. In this case, the spin precession axis coincides with the x axis of the structure and the spin rotation angle during electron motion is determined only by its displacement along the y-axis, Δy:

$$\theta = \frac{m\beta_1}{\hbar}\Delta y\,. \tag{64}$$

Notably, in this situation, the spin fluctuations in the different places are correlated or anticorrelated depending on the value of θ in Eqn (64) and independently of ballistic or diffusive electron motion. In this situation a persistent spin helix emerges [132–135]. If $\beta_1 = 0$, $\beta_2 \neq 0$, the spin helix forms not along the y-axis, but along the x-axis. The absence of the exact compensation of the structure and bulk asymmetries in the spin splitting, as well as the presence of terms cubic in the wave vector in the effective Hamiltonian, leads to the violation of relation (64), but, in a broad range of parameters, long-lived spin modes with nontrivial spin correlations are formed in two-dimensional structures.

A consistent theory of spin noise with spatial and time resolution is developed in Ref. [136] (see also review [137]), where experimental data concerning the observation of the spin helix in the spin diffusion are given. Spatio-temporal spin noise is characterized by the correlation function [cf. Eqn (4)]

$$\mathcal{K}_{\alpha\beta}(\boldsymbol{\rho},\tau) = \bigl\langle\{\delta s_\alpha(\mathbf{r}+\boldsymbol{\rho},t+\tau)\delta s_\beta(\mathbf{r},t)\}_\mathrm{s}\bigr\rangle\,, \tag{65}$$

where the averaging is performed over t and $\mathbf{r}$ (with fixed τ and $\boldsymbol{\rho}$). In the case of frequent collisions (61a), the authors of Ref. [136] derived the compact analytical expression for the Fourier transform of correlator (65):

$$\mathcal{K}_{\alpha\beta}(\mathbf{q},\omega) = \int\!\!\int \mathcal{K}_{\alpha\beta}(\boldsymbol{\rho},\tau)\exp(\mathrm{i}\omega\tau - \mathrm{i}\mathbf{q}\boldsymbol{\rho})\,\mathrm{d}\boldsymbol{\rho}\,\mathrm{d}\tau = \frac{mk_\mathrm{B}T}{16\pi\hbar^2}\left(\frac{1}{-\mathrm{i}\omega + \hat{\Gamma} + Dq^2 + \mathrm{i}2\tau^*\hat{\Lambda}(\mathbf{q})} + \mathrm{H.c.}\right)_{\alpha\beta}. \tag{66}$$

Here, D is the electron diffusion coefficient, $\hat{\Gamma}$ is the tensor of inverse spin relaxation times (61b), and the tensor $\hat{\Lambda}$ has the components

$$\Lambda_{\alpha\beta}(\mathbf{q}) = -\epsilon_{\alpha\beta\gamma}\hbar\int_0^{2\pi}\Omega_{\gamma,\mathbf{k}}(\mathbf{qk})\frac{\mathrm{d}\varphi_\mathbf{k}}{2\pi m^*}\,,$$

where $\varphi_\mathbf{k}$ is the polar angle of the vector $\mathbf{k}$. This tensor describes the electron spin precession and diffusion. The electron gas is assumed to be degenerate.

In Fig. 12 (a), a possible scheme is presented for the experimental detection of spatio-temporal spin noise in a structure with a quantum well, while panels (b–e) show the results of the calculation of the spatial distribution of the spin density correlation functions performed in Ref. [136]. One can distinctly see the spatial oscillations of the spin polarization even when the Rashba and Dresselhaus contributions to the spin splitting are considerably different. This is related to the fact, that, despite the many trajectories of electron propagation in the diffusive regime between the given positions, the main contribution to the spin correlator is given by the trajectories close to the rectilinear one.

Above, the situation where the spin splitting $\mathbf{\Omega}_\mathbf{k}$ does not depend on the coordinates was considered. There are a number of systems where the spin splitting of the bands is absent or is significantly suppressed 'on average', but the spatial fluctuations are still present (see review [138]). The spin dynamics in these systems can be considerably different from the case of coordinate independent spin splitting. One may expect that the spin noise in these systems will demonstrate a number of specific features as well. This question remains poorly investigated, but in quasi-one-dimensional systems with the spatial fluctuations of spin splitting, a power law divergence at low frequencies is expected [139].

Now, let us turn to a description of spin noise in two-dimensional systems out of thermal equilibrium. The role of spin-orbit interaction is particularly important if an external electric field $\mathbf{E}$ is applied to the system and causes electron drift. The nonzero average wave vector $\langle\mathbf{k}_\mathrm{dr}\rangle = (m\mu/\hbar)\,\mathbf{E}$, with μ being the mobility of the charge carriers, leads — due to spin-orbit interaction — to the nonzero average effective magnetic field, which causes the regular precession of the spin fluctuations with frequency $\mathbf{\Omega}_{\mathbf{k}_\mathrm{dr}}$. This results in a current induced shift of the peak in the spin noise spectrum. This effect was proposed and theoretically described in Ref. [140]. If the external magnetic field is absent, the peak in the spin noise spectrum is centered at the frequency $\Omega_{\mathbf{k}_\mathrm{dr}}$, or at the frequency $|\mathbf{\Omega}_{\mathbf{k}_\mathrm{dr}} + \mathbf{\Omega}_\mathrm{L}|$, with $\mathbf{\Omega}_\mathrm{L}$ being the Larmor spin precession frequency, if a magnetic field is present. Experimentally, an analogous effect was observed in electron spin resonance measurements in noncentrosymmetric SiGe quantum wells [141].

With an increase in electric current, the nonequilibrium effects in the spin noise spectra become even more pronounced [29]. The general theory of spin noise in such conditions is described in Ref. [33].

In Ref. [142], a microscopic theory of spin dynamics and fluctuations of electron gas is developed for the streaming

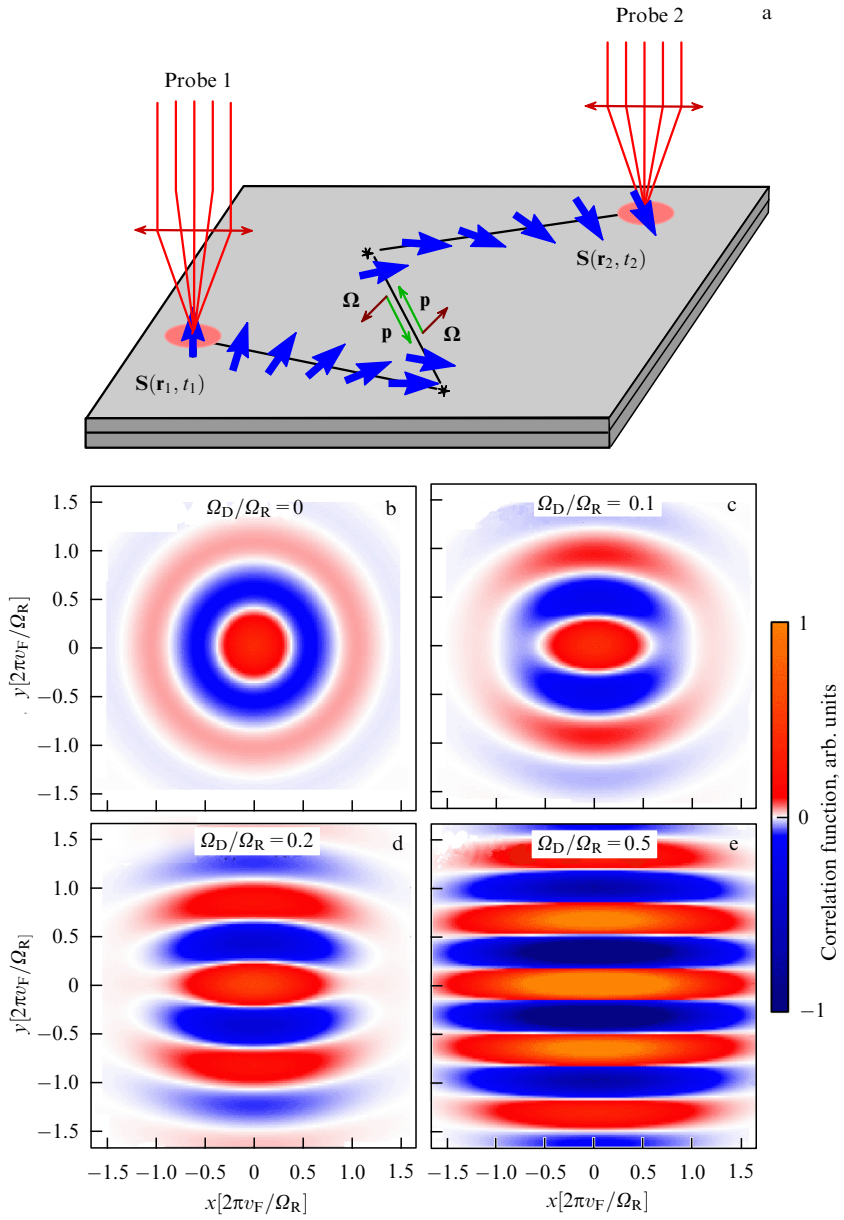

Figure 12. (a) Sketch of the possible experimental measurement of spatial correlation functions of spin density fluctuations in a quantum well. (b–e) Spatial dependence of the correlator of the normal component of spin density $\mathcal{K}_{zz}(\boldsymbol{\rho}, \tau)$ in the quantum well. Effective Rashba and Dresselhaus fields are introduced according to $\Omega_R = (\beta_1 - \beta_2)k_F/2$, $\Omega_D = (\beta_1 + \beta_2)k_F/2$. Calculations are performed for $\tau = 20/(\Omega_R^2\tau^*)$, $\Omega_R\tau^* = 0.2$, and various values of the Dresselhaus field. (Adapted from Ref. [136].)

regime taking into account the spin-orbit interaction. The streaming regime is realized in relatively clean semiconductor structures under the application of moderately strong electric fields. It is characterized by ballistic electron acceleration to the optical phonon energy during the time t_{tr}, followed by the emission of a phonon, loss of energy, and return to the region of small energies [143].

In Ref. [142] the kinetic equation is derived that describes the spin dynamics in the streaming regime taking into account the spin-orbit interaction. It turns out to be convenient to separate the region in the momentum space with the small momentum component in the direction perpendicular to the applied electric field (the so-called 'needle') from the rest of the momentum space. The dominant part of electrons in the streaming regime is in the 'needle'. Elastic scattering on impurities or quasielastic scattering on acoustic phonons leads to the scattering of electrons from the needle to the rest of the momentum space. The separation of the two contributions to the spin distribution function allows the description of the spin dynamics to be reduced to the determination of the spin noise spectrum and analysis of the eigenmodes in the system.

The damping rates of the different spin modes can be considerably different. Depending on the relation between Rashba and Dresselhaus spin splittings, the spin distribution in the momentum space can quickly relax to the homogeneous one (zeroth eigenmode) or to the oscillating one (one of the higher modes). In the latter case, a spin helix in the momentum space arises. The damping of the most long-lived spin mode can be determined by a combination of the spin-orbit coupling and the quasielastic scattering, in analogy with the Dyakonov–Perel mechanism [144], or by

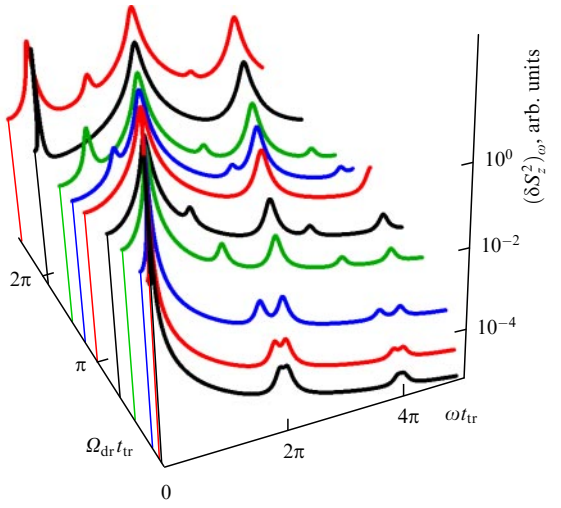

Figure 13. Electron spin noise spectra in the streaming regime for various values of the external electric field. (Adapted from Ref. [142].)

the electron penetration in the region, where the energy is larger than the optical phonon energy, depending on the system parameters.

The complex spin dynamics in the system manifests itself in the spin noise spectra. The noise spectrum consists of a series of peaks with their positions determined by the time of acceleration to the optical phonon energy $t_{tr} \propto 1/E$ and the average spin precession frequency in the spin-orbit field, Ω_{dr}. The shape of the spectra for different values of the parameter $\Omega_{dr}t_{tr}$ is shown in Fig. 13. The central frequencies and widths of the peaks are determined by the eigenfrequencies and decay times of the corresponding spin modes in the system. The dominant peak is centered at the frequency Ω_{dr}. However, in the case of $\Omega_{dr}t_{tr} = 2\pi k$, where k is an integer number, the spin helix in the momentum space emerges in the system, as mentioned above, and the electron spin rotates by an angle that is a multiple of 2π between the two consequent phonon emissions, independently of the number of elastic scatterings during this time. In this case, the amplitude of the peak at the lowest frequency drastically increases (see the black curve corresponding to $\Omega_{dr}t_{tr} \approx 2\pi$).

Apart from electron systems, exciton and exciton polariton systems are actively studied from the spin noise viewpoint. The key feature of these systems is the fact that they are fundamentally nonequilibrium, because excitons in quantum wells and exciton polaritons in quantum microcavities have finite lifetimes, so a considerable role in these systems is played by the pumping and fluctuations of a number of quasiparticles accompanying it (generation-recombination noise). Moreover, excitonic systems have a rich fine structure: in quantum wells, there are optically active (bright) excitons with a projection of the total angular momentum of the electron hole pair on the growth axis $m_z = \pm 1$, as well as dark states with $m_z = \pm 2$. In Ref. [32], the spin noise theory of bright and dark excitons is developed for quantum wells in a transverse magnetic field, and the interplay between electron-hole interaction leading to splitting between states with $|m_z| = 1$ and $|m_z| = 2$ and the external magnetic field-induced mixing of bright and dark states is analyzed. In Refs [145, 146], the spin noise of exciton polaritons is studied theoretically. Here, important effects are the deceleration of the noise due to the Bose stimulation effect, modification of spin noise statistics with an increase in the pump power [147], and the considerable role of particle-particle interactions [146]. It was shown theoretically and experimentally that, in structures with quantum microcavities, giant enhancement of the spin noise can take place due to the effects of optical instability [148].

6. High order spin correlators

In the previous sections, we considered the spin correlation functions of the second order only. These correlators carry information about the spin dynamics, but generally do not describe them completely. Complete information about spin properties is contained in the full set of correlators of all orders. For the classical fluctuating quantity $\mathbf{S}(\mathbf{t})$, the nth order correlator has the form

$$\left\langle \delta S_z(t_1)\, \delta S_z(t_2) \ldots \delta S_z(t_n) \right\rangle . \tag{67}$$

Generally, for quantum operator $\delta\hat{S}_z(t)$, this expression should be symmetrized [90]:

$$\left\langle \left\{ \delta\hat{S}_z(t_1) \{ \delta\hat{S}_z(t_2) \ldots \delta\hat{S}_z(t_n) \}_s \ldots \right\}_s \right\rangle , \tag{68}$$

cf. Eqn (4). Here, the order $t_1 < t_2 < \ldots < t_n$ is assumed, and, as above, we consider the thermal energy to be much larger than the Zeeman splitting of spin states, so there is no average spin polarization, $\langle S_z(t) \rangle = 0$, and all the correlators of odd order vanish.

For an ensemble of N independent spins, it is convenient to study, instead of correlation function (67), the cumulants [149–151]. They are defined by the generating function

$$\ln \left\langle \exp \left(\sum_{i=1}^{n} x_i\, \delta S_z(t_i) \right) \right\rangle . \tag{69}$$

In particular, the analog of Eqn (67) is the coefficient C_n of $x_1, x_2, \ldots, x_n$ in the decomposition of the generating function into Taylor series. For example, for $n = 2$ and $n = 4$, the cumulants have the form

$$C_2\{\delta S_z(t)\} = \left\langle \delta S_z(t_1)\, \delta S_z(t_2) \right\rangle , \tag{70a}$$

$$\begin{aligned} C_4\{\delta S_z(t)\} = {} & \left\langle \delta S_z(t_1)\, \delta S_z(t_2) \delta S_z(t_3)\, \delta S_z(t_4) \right\rangle \\ & - \left\langle \delta S_z(t_1)\, \delta S_z(t_2) \right\rangle \left\langle \delta S_z(t_3)\, \delta S_z(t_4) \right\rangle \\ & - \left\langle \delta S_z(t_1)\, \delta S_z(t_3) \right\rangle \left\langle \delta S_z(t_2)\, \delta S_z(t_4) \right\rangle \\ & - \left\langle \delta S_z(t_1)\, \delta S_z(t_4) \right\rangle \left\langle \delta S_z(t_2)\, \delta S_z(t_3) \right\rangle . \end{aligned} \tag{70b}$$

Generally, in each average, the products should be symmetrized similarly to Eqn (68).

The advantage of cumulants over the usual correlators is additivity, which can be seen from the generating function (69). For a total spin composed of N independent contributions $\mathbf{S}_k(t)$,

$$\mathbf{S}(t) = \sum_{k=1}^{N} \mathbf{S}_k(t) , \tag{71}$$

the cumulants are the sums of independent contributions as well:

$$C_n\{\delta S_z(t)\} = \sum_{k=1}^{N} C_n\{\delta S_{k,z}(t)\}\,. \tag{72}$$

It can be seen that, for $N \gg 1$, the dominant contribution to the correlator (67) is made by the second order cumulant, and the higher order cumulants can be ignored. Thus, the noise of many independent spins is Gaussian, which means that the high order correlators can be calculated using Wick's theorem.

The noise from a few spins is, generally, non-Gaussian. For example, for a single electron spin ($S = 1/2$), the same-time fourth order cumulant is not zero:

$$C_4 = \langle \delta S_z^4 \rangle - 3\langle \delta S_z^2 \rangle^2 = -\frac{1}{8}\,. \tag{73}$$

For different times $t_1 < t_2 < t_3 < t_4$, the cumulant is given by

$$C_4\{\delta S_z(t)\} = -\langle \delta S_z(t_1)\,\delta S_z(t_3)\rangle\langle \delta S_z(t_2)\,\delta S_z(t_4)\rangle - \langle \delta S_z(t_1)\,\delta S_z(t_4)\rangle\langle \delta S_z(t_2)\,\delta S_z(t_3)\rangle\,. \tag{74}$$

The cumulant of the nth order depends on $n-1$ time intervals, so its spectrum depends on $n-1$ frequencies. The simplest illustration of a spectrum of the high order is the bispectrum, which is a section of the fourth order spin noise spectrum. It is defined as a Fourier transform of the correlator (70b) at the times $t_1 = t$, $t_2 = t + \tau_1$, $t_3 = t + \tau$, $t_4 = t + \tau + \tau_2$, integrated over τ:

$$B(\omega_1, \omega_2) = \int\int \mathrm{d}\tau_1\,\mathrm{d}\tau_2 \exp(\mathrm{i}\omega_1\tau_1 + \mathrm{i}\omega_2\tau_2) C_4(\tau_1, \tau_2)\,, \tag{75}$$

where

$$C_4(\tau_1, \tau_2) = \int \mathrm{d}\tau\, C_4\{\delta S_z(t)\,\delta S_z(t+\tau_1) \times \delta S_z(t+\tau)\,\delta S_z(t+\tau+\tau_2)\}\,. \tag{76}$$

The bispectrum reflects the correlation degree of the spin noise at the frequencies ω_1 and ω_2. In the calculation of the bispectrum of the quantum noise, the operators should be symmetrized as in Eqn (68). As a result, for an ensemble of electrons, using Eqn (74), we obtain

$$NC_4(\tau_1, \tau_2) = -(|\tau_1| + |\tau_2|)C_2(\tau_1)C_2(\tau_2) - \int_{-\infty}^{\infty} \big[C_2(\tau - |\tau_2|)\,C_2(\tau + |\tau_1|) + C_2(|\tau| + |\tau_1|)\,C_2(|\tau| + |\tau_2|)\big]\,\mathrm{d}\tau\,, \tag{77}$$

where

$$C_2(\tau) = \langle \{\delta S_z(t)\,\delta S_z(t+\tau)\}_s \rangle\,. \tag{78}$$

Provided the spin fluctuations precess in a transverse magnetic field with the frequency Ω_L and relax during time τ_s (as in the derivation of Eqn (9)), the bispectrum at positive ω_1 and ω_2 has the form

$$NB(\omega_1, \omega_2) = \frac{\tau_s^3\big[(\delta_1 + \delta_2)^2 + 4\big](\delta_1\delta_2 - 1)}{16(1 + \delta_1^2)^2(1 + \delta_2^2)^2}\,, \tag{79}$$

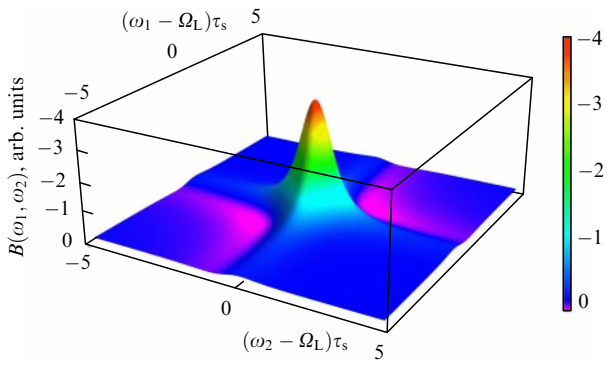

Figure 14. (Color online.) Spin noise bispectrum in a transverse magnetic field, calculated from Eqn (79). Vertical axis is directed downwards for better visibility, so the small positive values of $B(\omega_1, \omega_2)$ are shown by magenta areas.

where $\delta_{1,2} = (\omega_{1,2} - \Omega_L)\tau_s$ and it is assumed that $\Omega_L\tau_s \gg 1$. This expression is shown in Fig. 14. The bispectrum is centered at $\omega_1 = \omega_2 = \Omega_L$, and in the region where $\omega_1 - \Omega_L$ and $\omega_2 - \Omega_L$ have the same sign, the bispectrum can be positive, and it is negative in the other region. These cases can be interpreted as positive and negative correlations between the noise at frequencies ω_1 and ω_2 [20].

The approach described above is valid for describing so-called 'weak' quantum mechanical measurements, when the measurement hardly changes the density matrix of the system [152]. The finite strength of the measurement can be described using the Krauss operators [153, 154]

$$K(s) = \left(\frac{2\lambda}{\pi}\right)^{1/4} \exp\big[-\lambda(s - S_z)^2\big]\,, \tag{80}$$

where S_z is the spin operator, s is the continuous real parameter, and λ describes the measurement strength. The probability of the spin measurement is $1 - \exp(-\lambda/2)$. After a pulsed measurement, the density matrix takes the form

$$\rho(s) = K(s)\rho K(s)\,, \tag{81}$$

and it freely evolves between the measurements. After n measurements, the average of the spin correlation function can be found as

$$\langle S_z(t_1)S_z(t_2)\ldots S_z(t_n)\rangle = \iint\ldots\int s_1 s_2 \ldots s_n \,\mathrm{Tr}\big[\rho(s_1, s_2, \ldots, s_n)\big]\mathrm{d}s_1\,\mathrm{d}s_2\ldots\,\mathrm{d}s_n\,, \tag{82}$$

where the parameters s_i $(i = 1, 2, \ldots, n)$ characterize measurements at times t_i.

In the limit of weak measurements, when the parameter $\lambda \to 0$, this definition of the correlation function coincides with Eqn (68) [155]. In the limit of the strong measurements ($\lambda \to \infty$), the correlator can be rewritten as

$$\langle S_z(t_1)S_z(t_2)\ldots S_z(t_n)\rangle = \sum_{m_1 m_2 \ldots m_n} m_1 m_2 \ldots m_n \times \mathrm{Tr}\big[P_{m_n} U_{t_n - t_{n-1}}\big(P_{m_{n-1}} \times U_{t_{n-1} - t_{n-2}}(\ldots U_{t_2 - t_1}(P_{m_1}\rho P_{m_1})\ldots)P_{m_{n-1}}\big)P_{m_n}\big]\,, \tag{83}$$

where m are the eigenvalues of the operator S_z, P_m are the projectors on the corresponding eigenstates ($S_z = \sum_m mP_m$), and superoperator $U_\tau(\rho)$ describes the free evolution of the density matrix during time τ. In fact, this expression (83) describes the average over all possible trajectories of the system evolution among spin values m_i at time moments t_i, and with each measurement the density matrix of the system is projected to the corresponding state (eigenvalues m_i are assumed to be nondegenerate).

As a simple nontrivial example illustrating the difference between strong and weak measurements from the point of view of spin noise spectroscopy, one can consider the correlators of spin S in a transverse magnetic field. The second order correlator does not depend on the measurement strength λ and can be calculated using the methods described in Section 2. For $S = 1/2$, the fourth order correlator does not depend on λ either. However, the difference shows up for $S = 1$. For example, for three equal time intervals, one can show that

$$\left\langle \delta S_z(0)\,\delta S_z(\tau)\,\delta S_z(2\tau)\,\delta S_z(3\tau)\right\rangle = \frac{1}{36}\left[16\cos^2(\Omega_L\tau)\right.$$
$$\times \exp\left(-\frac{2\tau}{\tau_s}\right) + \exp\left(-\frac{3\tau}{\tau_s}\right) + \cos(2\Omega_L\tau)\exp\left(-\frac{3\tau}{\tau_s}\right)$$
$$\left. + 6\cos(4\Omega_L\tau)\exp\left(-\frac{3\tau}{\tau_s}\right)\right], \qquad (84a)$$

$$\left\langle \delta S_z(0)\,\delta S_z(\tau)\,\delta S_z(2\tau)\,\delta S_z(3\tau)\right\rangle_{\text{strong}} = \frac{1}{18}\cos^2(\Omega_L\tau)$$
$$\times \exp\left(-\frac{2\tau}{\tau_s}\right)\left[8 + \exp\left(-\frac{\tau}{\tau_s}\right) + 3\cos(2\Omega_L\tau)\exp\left(-\frac{\tau}{\tau_s}\right)\right], \qquad (84b)$$

where the first expression describes the 'usual' correlator (68), which corresponds to the weak measurements, and the subscript 'strong' corresponds to the limit $\lambda \to \infty$. The spin relaxation here is described in the 'τ-approximation' for the density matrix. These correlators are shown in Fig. 15 by the black solid (*1*) and red dashed (*2*) lines, respectively.

In the limit of many particles, the spin noise is Gaussian, so the fourth order cumulant vanishes and the fourth order correlator reduces to the sum of the products of the second order correlators (see Eqn (70b)). In this case, we obtain (the spectrum is normalized by the number of spins)

$$\left\langle \delta S_z(0)\,\delta S_z(\tau)\,\delta S_z(2\tau)\,\delta S_z(3\tau)\right\rangle_{\text{Gauss}} = \frac{1}{9}\left[2\cos^2(\Omega_L\tau)\right.$$
$$\times \exp\left(-\frac{2\tau}{\tau_s}\right) + \exp\left(-\frac{4\tau}{\tau_s}\right) + \cos(2\Omega_L\tau)$$
$$\left. \times \exp\left(-\frac{4\tau}{\tau_s}\right) + 2\cos(4\Omega_L\tau)\exp\left(-\frac{4\tau}{\tau_s}\right)\right]; \qquad (85)$$

this expression is shown by the blue dotted curve (*3*) in Fig. 15.

In the case of the usual Faraday rotation measurement for a single spin, the parameter λ can be estimated as $\overline{N}\theta_F^2$ [91], where $\overline{N}$ is the average number of photons in the probe pulse and θ_F is the Faraday rotation angle for completely polarized spin. For typical experiments, the authors of Ref. [91] give the estimate $\lambda \sim 10^{-4}$. Measuring the high order spin correlators

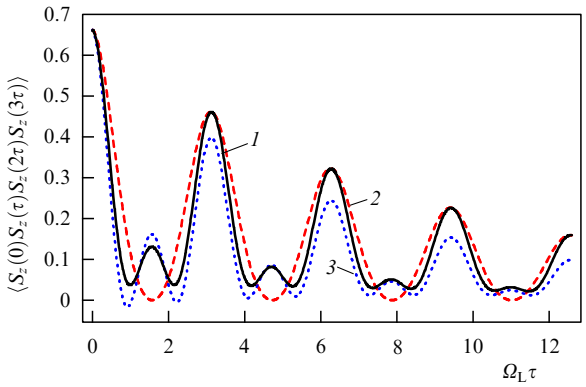

Figure 15. (Color online.) Fourth order correlator of a single spin $S = 1$ for weak measurements (black solid curve *1*, Eqn (84a)), strong measurements (red dashed curve *2*, Eqn (84b)), and a large ensemble of spins $S = 1$ (blue dotted curve *3*, Eqn (85)).

allows one, for example, to distinguish between homogeneous and inhomogeneous broadening of the spin resonances (spin dephasing and decoherence times) [91, 156, 157], to study the properties of the reservoir, which leads to spin relaxation [158, 159], and to study the effects of the interaction, which are not accessible from the second order correlator [160]. For electrons localized in quantum dots, the measurement of the fourth order spin correlators allows obtaining the parameters of the nuclear spin dynamics caused by precession in the external magnetic field or in the Knight field or by the interaction of the nuclear quadrupole moment with the elastic strain in the quantum dot [161, 162].

In the case of monoexponential spin relaxation, the usual spin noise spectrum consists of a series of Lorentzian peaks with the corresponding widths centered at the eigenfrequencies of the system (see Eqn (27)). Interestingly, the decomposition of the free energy into powers of the spin operator allows one to show that the spectra of the correlators of high orders are also described by universal expressions with a small set of parameters [163]. The same approach allows the use of the time reversal symmetry to establish the general relations between the spin correlation functions of high orders and nonlinear spin susceptibility or the dependence of the lower order spin correlators on the magnetic field [20, 64].

Typically, the spin noise is not measured using probe pulses, but using continuous light. In this case, spin measurements at intermediate times do not directly contribute to correlator (82), but modify the density matrix [91, 200]. This was demonstrated in measurements of the second order spin correlation function for a single quantum dot [157]. Thus, for example, if strong spin measurements are performed at the time moment τ between the two other spin measurements at times 0 and t ($0 < \tau < t$), then the correlator takes the form

$$\left\langle S_z(0)S_z(t)\right\rangle_\tau = 4\left\langle S_z(0)S_z^2(\tau)S_z(t)\right\rangle, \qquad (86)$$

where the spin 1/2 is considered. For the strong intermediate measurement, this correlator is generally different from $\langle S_z(0)S_z(t)\rangle$ [161, 162].

In the limit of strong continuous measurements, the spin dynamics are almost frozen due to the quantum Zeno effect, as described in Section 3.5. The spin noise in these conditions is the telegraph noise: at each moment, the spin is in one of the eigenstates [89].

In conclusion, we note that the direct measurement of the high order spin correlators is challenging, and a number of alternative detection methods are suggested. For example, to overcome the parametric suppression of the high order cumulants for many spins, one can study the 'stimulated' spin noise [165], when an external magnetic field [166] or optical orientation synchronizes single spins, so that they are no longer independent. The other possibility of high order spin noise measurement is due to the nonlinear relation between the detected Faraday rotation angle and the spin polarization. This method allowed the authors of Ref. [167] to observe the noise of optical alignment in atomic gases. The same method allows one to study the spin correlators of high orders for spins that do not directly participate in optical transitions [168]. Such spins can be provided by the host lattice nuclei, magnetic impurities, and nuclei of donors and acceptors, which created electron or hole bound states [169, 170].

In typical experimental conditions, the dominant mechanism of the Faraday rotation by nuclear spin fluctuation $\delta\mathbf{I}$ is related to the splitting of the trion resonance frequency ω_0 by $2a\delta I_z$ due to the hyperfine interaction [65, 168] (a is the real constant; see also Section 7). For $\sigma^{\pm}$ polarized light at frequency ω, the contribution to the transmission coefficient caused by a single resonance has the form

$$t_{\pm} \propto \frac{1}{\omega - \omega_0 \mp a\delta I_z + \mathrm{i}\gamma}\,, \tag{87}$$

where γ is the homogeneous resonance linewidth. The Faraday rotation angle is determined by the difference between the phases of the transmitted circularly polarized components and has the form

$$\theta_{\mathrm{F}} \propto \mathrm{Im}\left[(t_+ - t_-)t^*\right] \propto \frac{a\delta I_z \gamma}{(\omega - \omega_0)^2 + \gamma^2}\,, \tag{88}$$

where $t = (t_+ + t_-)/2$, and we took into account the fact that $a\delta I_z \ll \gamma$. We can see that, in contrast to Faraday rotation by spin noise of the resident charge carriers (18), this effect is the strongest exactly at the resonance ($\omega = \omega_0$). To describe the Faraday rotation in realistic systems, Eqn (88) can be averaged over the inhomogeneous broadening of the resonance. Alternative mechanisms of the Faraday rotation are variations of the thermal occupancies of the electron spin sublevels and contributions from the interband transitions [169, 170].

For example, at zero detuning, $\omega = \omega_0$, the Faraday rotation signal (see Eqns (18) and (88)) can be presented as

$$\mathcal{F} = \mathrm{Re}\left\{\delta P_y E^*_{0,x}\right\} = C\sum_{n=0}^{\infty}\left(\frac{a\delta I_z}{\gamma}\right)^{2n+1}, \tag{89}$$

where C is a real constant. This expression shows that even the second order correlation function of the Faraday rotation contains contributions from the spin correlation functions of high orders:

$$\left\langle \mathcal{F}(0)\mathcal{F}(\tau)\right\rangle = C^2\sum_{n,n'}\left(\frac{a}{\gamma}\right)^{2(n+n'+1)}\left\langle \delta I_z^{2n+1}(0)\,\delta I_z^{2n'+1}(\tau)\right\rangle. \tag{90}$$

The drawback of this approach is the possibility of measuring the spin correlators related to the two time moments 0 and τ only.

7. Extensions of spin noise spectroscopy

Most often, spin noise spectroscopy, as described above, is used to study the spin properties of electrons and holes. At the same time, Faraday rotation can be induced by any physical quantity, which transforms under symmetry operations in the same way as the component of the pseudovector S_z. In this section, we describe the capabilities to detect fluctuations of the host lattice nuclear spins, magnetic impurities, electric charges in a magnetic field, valley polarization, and electric current in gyrotropic systems. Apart from that, we discuss opportunities to study optical spectra and spatial correlations of spin noise, which have been realized experimentally in the past few years.

Spins of the host lattice nuclei do not directly participate in interband optical transitions. However, the mechanism of the Faraday rotation for nuclei discussed in the previous section allows one to detect their spin noise. For example, in Fig. 16, we show the Faraday rotation noise spectrum for bulk GaAs doped with Si for the frequency of the probe beam in the vicinity of the trion resonance for donors. The peaks at the spin precession frequencies of nuclei of ^{69}Ga, ^{71}Ga, and ^{75}As can distinctly be seen [65]. In this system, the hyperfine interaction with the resident electron and hole in trion leads to a shift of the trion resonance by

$$a\delta I_z = \frac{1}{\hbar}\left(\frac{1}{2}A^{\mathrm{e}} + \frac{3}{2}A^{\mathrm{h}}\right)\sum_{k=1}^{N_{\mathrm{n}}}\delta I_{k,z}\,, \tag{91}$$

as discussed in the previous Section 6. Here, the hyperfine interaction constants for an electron, A^{e}, and hole, A^{h} in trion, are assumed to be equal for all nuclei in the vicinity of the donor [cf. Eqn (20)]. Similarly, the hyperfine interaction allows one to detect the spin noise of magnetic impurities, for example, manganese [168, 171].

Nuclear spin noise spectra can be calculated, for example, in the framework of the central spin model (see Section 3.1)

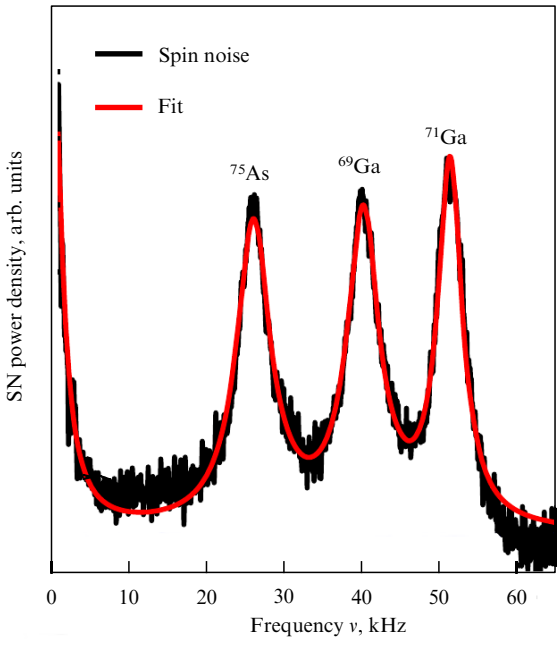

Figure 16. Nuclear spin noise spectrum detected in the vicinity of trion resonance for electrons bound at Si donors in bulk GaAs in a transverse magnetic field of 3.75 mT. (Adapted from Ref. [65].)

[46, 172]. The spin noise spectrum of nuclei with $I = 1/2$ in a strong transverse magnetic field has the form [57]

$$\left\langle \delta I_z^2 \right\rangle_\omega = \frac{\pi\hbar N_\mathrm{n}}{2}\,\mathcal{P}\left(|2\hbar\omega - \mu_\mathrm{n} g_\mathrm{n} B|\right), \tag{92}$$

where $\mathcal{P}(A)$ is the distribution function of the hyperfine interaction constants. Thus, the shape of the spin noise spectrum, in contrast to the electron spin noise spectrum, allows determining the distribution function not of the Overhauser field but of the Knight field.

This approach allows us to study the nuclear spin dynamics at the submillisecond time scale. However, the nuclear spin dynamics can take place at a time scale of the order of minutes, or even hours in the case of dynamic nuclear polarization or relaxation of nuclear polarization. Since the rate of energy transfer between nuclear spins is much faster than that between nuclei and the host lattice or resident electrons, the nuclear spin system can be described using the effective nuclear spin temperature $\Theta_\mathrm{N}(t)$, which slowly varies with time. In realistic systems, this temperature can be smaller than that of the host lattice by a few orders of magnitude and can be positive or negative [38].

To study experimentally the nuclear spin dynamics, at the first stage, the nuclei should be dynamically polarized in a longitudinal magnetic field using a strong circularly polarized beam, which induces interband transitions in the semiconductor. At the second stage, the optical excitation should be switched off and the magnetic field can be optionally reoriented. Nuclear spin temperature $\Theta_\mathrm{N}(t)$ slowly relaxes with laboratory time t to the lattice temperature, and the electron spin noise of resident electrons is measured during this time. In a transverse magnetic field (Voight geometry), the precession peak in the spin noise spectrum is centered at the frequency $\mathbf{\Omega}_\mathrm{tot}(t) = \mathbf{\Omega}_B + \overline{\mathbf{\Omega}}_\mathrm{N}(t)$ [cf. Eqn (9b)]. Here,

$$\overline{\mathbf{\Omega}}_\mathrm{N}(t) = \frac{AI}{\hbar}\frac{\mathbf{B}}{B}\mathcal{B}_I\left(\frac{\mu_\mathrm{n} g_\mathrm{n} BI}{k_\mathrm{B}\Theta_\mathrm{N}(t)}\right) \tag{93}$$

is the spin precession frequency in the Overhauser field averaged over the ensemble [1], where A is the hyperfine interaction constant, I is the nuclear spin, $\mathcal{B}_I(x)$ is the Brillouin function, and μ_n and g_n are the nuclear magneton and g-factor, respectively.

Since the nuclear spin temperature $\Theta_\mathrm{N}(t)$ relaxes to the host lattice temperature, measuring the electron spin noise spectrum with the time resolution allows one to study nonequilibrium nuclear spin polarization in the absence of external excitation [78]. This proposal was realized experimentally [173, 174]. The theoretical and experimental results are shown in Fig. 17 in panels (a, c) and (b, d), respectively. The color shows the intensity of the nuclear spin noise at the given frequency at the given time moment. Depending on the sign of the nuclear spin temperature, the spin precession frequency $\Omega_\mathrm{tot}(t)$ can either always remain positive (Fig. 17a, b) or cross zero (Fig. 17c, d). Interestingly, the electron excitation by circularly polarized light creates for them an effective longitudinal magnetic field due to the dynamic Zeeman effect [174]. The width of the precession peak, as mentioned in Section 3, generally depends on the nuclear polarization degree [78].

Similarly to the nuclear spin polarization, an external magnetic field **B** also leads to the Faraday rotation described by Eqn (88), where the role of the splitting $2a\delta I_z$ is played by $(g_\mathrm{e} - g_\mathrm{h})\mu_\mathrm{B} B_z/\hbar$ (g_e and g_h are g-factors of the electron and hole in trion). This Faraday rotation takes place only if the

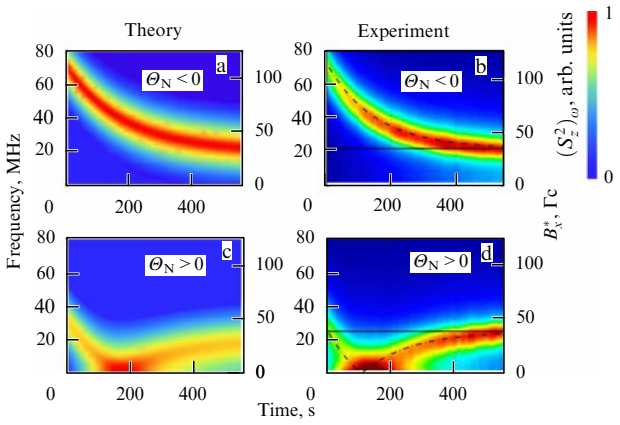

Figure 17. (Color online.) Time resolved spin noise spectra of electrons, interacting with nonequilibrium nuclear spin polarization perpendicular to the probe beam propagation direction. (a, b) Negative, (c, d) positive nuclear spin temperatures. Panels (a), (c) and (b), (d) show theoretical and experimental results, respectively. (Adapted from Ref. [174].)

localized state is occupied with a single charge carrier. If the occupancy of the state can take two values, $n = 0, 1$, its fluctuations δn lead to the noise of the Faraday signal:

$$\delta\theta_\mathrm{F} \propto \frac{B_z\gamma}{(\omega - \omega_0)^2 + \gamma^2}\,\delta n\,. \tag{94}$$

In Fig. 18, we show the spectra of Kerr rotation measured for a single quantum dot [175, 176]. Far from the resonance (Fig. 18a), the spectrum consists of a peak at the zero frequency, which corresponds to the hole spin noise. With the approach of the resonance (Fig. 18b), this peak broadens (see Section 3.5) and, in agreement with Eqn (94), a new peak appears, which is related to fluctuations of the quantum dot occupancy (blue curve *1*). A detailed analysis of the spectra allows one to determine the Auger recombination rate of the trion in addition to the parameters of the spin dynamics.

Additional extensions of the spin noise spectroscopy are provided by the spin-orbit interaction, which can lead to the lifting of spin degeneracy in many-valley semiconductors. In this case, the time reversal symmetry relates the Bloch wave vector with the opposite one, so all the states remain twofold degenerate, in agreement with the Kramers theorem. A pair of degenerate states can be characterized by the valley pseudospin $\boldsymbol{\tau}$. Thus, in many-valley semiconductors, the Faraday rotation noise spectrum consists of two contributions,

$$(\delta\theta_\mathrm{F}^2)_\omega = A\,(\delta S_z^2)_\omega + B\,(\delta\tau_z^2)_\omega\,, \tag{95}$$

which describe the spin and valley noise, respectively (there can also be a contribution from the cross-correlation functions $\langle\delta S_z(t)\delta\tau_z(t')\rangle$). A microscopic theory of this effect was developed for transition metal dichalcogenide monolayers [177], and the valley noise was measured [178].

The spin-orbit interaction can also lead to the locking of the spin direction with the direction of electron propagation. A classical example is bulk tellurium, where the current flow leads to spin polarization and induces optical activity [179–181]:

$$\theta_\mathrm{F} \propto j_z \propto S_z\,, \tag{96}$$

where the z-axis is the main axis of the crystal and also the light propagation direction. In this case, the Faraday rotation

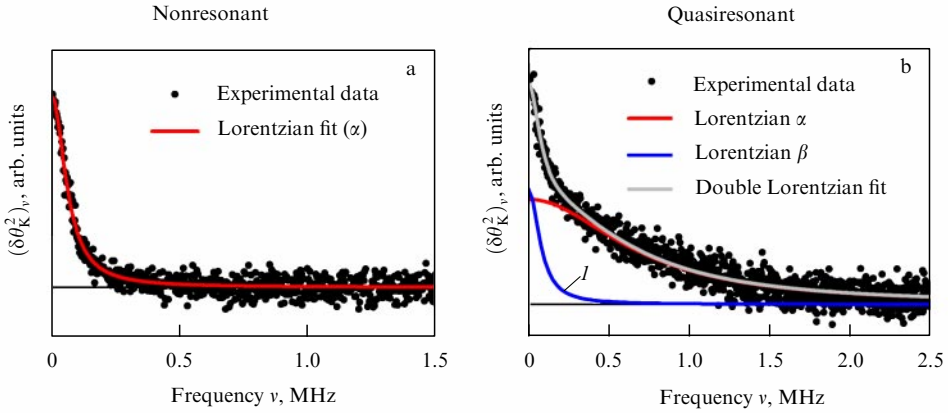

Figure 18. (Color online.) Kerr rotation noise spectra for (a) $|\omega - \omega_0| \gg \gamma$ and (b) $|\omega - \omega_0| \ll \gamma$ in external longitudinal magnetic field $B_z = 31$ mT, measured for a single In(Ga)As quantum dot. Blue curve *1* shows the contribution from the quantum dot occupancy noise. (Adapted from Ref. [175].)

noise spectrum is determined by the current noise spectrum [182]. Effects of this kind are possible in any gyrotropic system, for example, for ensembles of chiral nanotubes [183] and GaAs-based quantum wells with the crystallographic orientation [001] for the oblique incidence of light [184] (in this case, the contribution of the spin current noise is also possible). An illustrative example is given by quantum wells with the [110] crystallographic orientation with the C_{2v} point symmetry group, where the spin-orbit interaction Hamiltonian allows for contributions of the form [123, 185]

$$\mathcal{H}_{SO} = \beta_e \sigma_z^{(e)} k_x^e + \beta_h \sigma_z^{(h)} k_x^h \,. \tag{97}$$

Here, $\beta_{e,h}$ are the parameters of the spin-orbit interaction for the lowest electron and hole subbands, $\sigma_z^{(e,h)}$ are the Pauli matrices acting of the pseudospin, and $k_x^{e,h}$ are the components of the corresponding wave vectors ($x \parallel [\bar{1}10]$, $y \parallel [001]$). From this expression (97), one can see that k_x transforms in the same way as σ_z, so fluctuations of the current along the x-axis can lead to the rotation of the polarization plane of the incident light along with the spin noise. After reflection of the incident wave, the polarization conversion is determined by the off-diagonal reflection coefficient [182]

$$r_{xy} = -r_{yx} = P_s s_z + P_j j_x \,, \tag{98}$$

where **s** and **j** are the spin and current densities, respectively, and the coefficients P_s and P_j in the spectral range around the transition between the lowest electron and hole subbands are

$$P_s = \frac{2\pi\omega|d|^2}{c\,(E_0 - \hbar\omega)} \,, \quad P_j = \frac{\pi\omega|d|^2\beta m}{ec\hbar(E_0 - \hbar\omega)^2} \,. \tag{99}$$

Here, d is the transition dipole moment, E_0 is the transition energy (damping is ignored), $\beta = \beta_e - \beta_h$, c is the speed of light, m is the electron effective mass, and the valence band is assumed to be completely occupied. Thus, the Kerr rotation noise spectrum consists of contributions from the spin noise, current noise, and cross-correlations. In this case, in the vicinity of the resonance, the dominant contribution is related to the current noise, and, far from the resonance, to the spin noise.

The measurement of the Faraday rotation noise intensity as a function of the detection frequency ω is termed optical spin noise spectroscopy [186]. This method allows one to separate the different contributions to the noise of optical signals and to distinguish between homogeneous and inhomogeneous broadenings of the optical resonances. Indeed, in the case of homogeneous broadening, the noise intensity is proportional to the squared Faraday rotation,

$$\langle \delta\theta_F^2 \rangle \propto \frac{(\omega - \omega_0)^2}{(\omega - \omega_0)^2 + \gamma^2} \langle \delta S_z^2 \rangle \,, \tag{100}$$

(see Eqn (18)), and has a dip in the resonance frequency at $\omega = \omega_0$. If inhomogeneous broadening with the typical width $\Delta\omega_0$ is present in the system, then this expression should be averaged with the corresponding distribution. For example, for Gaussian broadening with $\Delta\omega_0 \gg \gamma$, we obtain

$$\langle \delta\theta_F^2 \rangle \propto \exp\left(-\frac{(\omega - \omega_0)^2}{\Delta\omega_0^2} \right) \langle \delta S_z^2 \rangle \,, \tag{101}$$

so the noise intensity is highest at the center of the inhomogeneously broadened line. Interestingly, in atomic vapors, where the inhomogeneous broadening is provided by the Doppler effect, there can be a dip in the center of the inhomogeneously broadened line, similarly to the case of homogeneous broadening, which is caused by the fast momentum relaxation of atoms [187].

It is noteworthy that the proportionality between the spin noise intensity and the number of charge carriers in the probed volume (see, for example, Eqn (63)) allows one to determine the distribution of the concentration of the charge carriers by moving the focus of the laser beam [188].

Two probe beams instead of one allow one to analyze the cross-correlations of the Faraday rotation for the two beams [189, 190]. These fluctuations are largest when the two beams are crossed [18, 191], but even in the absence of intersection, the cross-correlations can take place due to the ballistic or diffusive propagation of electrons from one place to another [133, 192] (see Section 5). Measurements of this kind allow one to study the spin dynamics, not only with time resolution, but also with spatial resolution, and to determine, for example, parameters of the spin-orbit interaction for electrons and holes in the quantum wells.

Presently, a few experimental groups are studying the possibility of the spatial resolution of spin noise based on the close relation of spin noise spectroscopy with Raman spin-flip scattering (see Section 2.3). In this way, the interference is

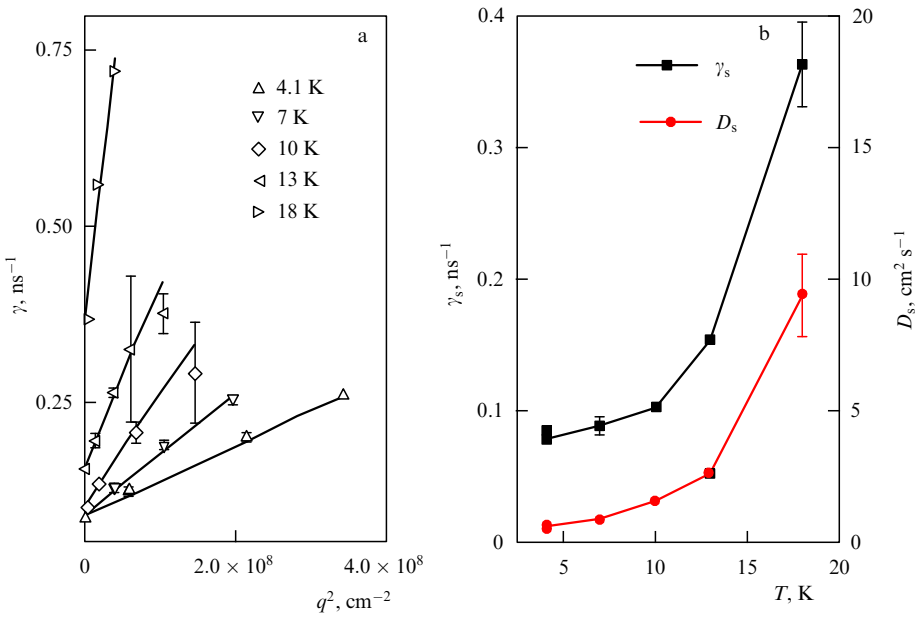

Figure 19. (Color online.) Width of spin noise spectrum $(\delta S_z^2)_{\omega,q}$ as a function of (a) q and (b) temperature, measured for bulk n-type CdTe. Red dots in Fig. b show the electron spin diffusion coefficient determined from these measurements. (Adapted from Ref. [193].)

studied between the probe light after propagation through the sample and the additional (reference) beam, which homo- or heterodynes the signal [193, 194]. In this case, the Stokes parameter, that is proportional to the Faraday rotation angle (see Eqn (18)), has the form

$$\delta\xi_1(t) = \frac{2\,\mathrm{Re}\,[\delta E_y^{\mathrm{pr}}(t) E_{0,x}^*]}{|E_{0,x}|^2}\,, \tag{102}$$

where the probe and reference beams are polarized along the x-axis, $E_{0,x}$ is the amplitude of the reference beam, and E^{pr} is the amplitude of the beam transmitted through the sample, and it is assumed that $E_{0,x} \gg E^{\mathrm{pr}}$. Experimentally, this method can be used to increase the sensitivity of the spin noise measurement [195] and to analyze high-frequency spin noise [37]. Importantly, after the scattering of the probe beam with the change in the wave vector by $\mathbf{q}$, the Faraday rotation is determined, not by the total spin fluctuation, but by its spatial harmonic $\delta S_z(t,\mathbf{q})$ [193]:

$$\delta\xi_1(t) \propto \int \delta s_z(t,\mathbf{r}) \exp(-\mathrm{i}\mathbf{q}\mathbf{r})\,\mathrm{d}\mathbf{r} \equiv \delta S_z(t,\mathbf{q})\,. \tag{103}$$

For example, provided the spin dynamics are characterized by spin relaxation time τ_s and the diffusion coefficient D_s, the Faraday rotation noise spectrum has the usual form:

$$(\delta S_z^2)_{\omega,q} = \frac{\tau/2}{1+(\omega\tau)^2} \tag{104}$$

(cf. (9a)); however, its width depends on the wave vector:

$$\frac{1}{\tau} = \frac{1}{\tau_s} + D_s q^2\,. \tag{105}$$

Measurements of this kind allow studying the transition from localized to free electrons with an increase in temperature via a change in the diffusion coefficient [63, 196]. An example of the experimental measurement of the width of the spin noise spectrum as a function of wave vector and of the temperature dependence of the diffusion coefficient is shown in Fig. 19 for the case of electrons localized at donors in bulk cadmium telluride.

8. Conclusions

The theory of spin noise in low dimensional systems and bulk semiconductors is reviewed. Spin noise in such systems is usually detected by fluctuations of the Faraday rotation of a continuous probe beam. General theoretical approaches were illustrated by a number of experimental results for structures of various dimensionality from 0D to 3D. At the same time, the review contains a number of original results concerning the influence of electrons tunneling on spin noise spectra and many-body spin localization (Section 3.4), spin fluctuations in 1D systems (Section 4), and the calculation of fourth order spin correlators depending on the strength of measurements (Section 6).

Further perspectives on the development of the spin noise spectroscopy method follow from Sections 6 and 7. They are related, first, to the analysis of high order spin correlations; second, to the development of the experimental technique for measuring spin noise with the spatial resolution; and third, to the measurement of the charge and valley fluctuations of charge carriers in semiconductors. Moreover, as the sensitivity in the experiments can be increased by homo- and heterodyne detection [37, 195] and by using squeezed light [197], it seems promising to combine these two experimental methods. Optomechanical resonances can also be applied to increase the noise signal, as was previously done in magnetometry [198].

The manifestation of quantum back action when making spin noise measurements is still not well understood. In spite of the fact that the quantum Zeno effect has probably already been observed experimentally [83], its microscopic description and the link between the strength of measurements and the measured spin signal is still not clear [89]. A fundamental challenge for the theory is the description of spin fluctuations in mesoscopic systems. Nowadays, the existing models can

describe only spin noise spectra for a small number of spins or for a large ensemble of spins. In the mesoscopic case, for example, when the spin of an electron interacts with several tens of nuclei or magnetic impurities, the theory remains undeveloped, and theoretical predictions of new effects in such systems are not yet available. Another problem deals with describing spin noise in nonlinear systems, for example, in the vicinity of a phase transition or upon formation of spin polarons [199]. Nonlinear equations of motion can also describe the nuclear field that acts on the localized electrons, as it is a classical quantity, not a quantum one.

The evolution of the theory of spin fluctuations is mostly determined by technological progress and the appearance of new systems in which new unexpected effects are predicted and observed. From this point of view, one of the most promising systems for further investigation of spin noise is twisted Van-der-Waals structures based on monolayers of transition metal dichalcogenides, as well as perovskites, topological insulators, Weyl semi-metals, and organic semiconductors.

Acknowledgments

The authors are thankful to V S Zapasskii and G G Kozlov for the fruitful discussions and careful reading of the review. The research was funded by RFBR, project number 19-12-50293.

References

1. Glazov M M *Electron and Nuclear Spin Dynamics in Semiconductor Nanostructures* (New York: Oxford Univ. Press, 2018)
2. Landau L D, Lifshitz E M *Statistical Physics* Pt. 1 (Oxford: Pergamon Press, 1980); Translated from previous Russian ed.: *Statisticheskaya Fizika* Ch. 1 (Moscow: Fizmatlit, 2005)
3. Lifshitz E M, Pitaevskii L P *Physical Kinetics* (Oxford: Pergamon Press, 1981); Translated from previous Russian ed.: *Fizicheskaya Kinetika* (Moscow: Fizmatlit, 2007)
4. Aleksandrov E B, Zapasskii V S *Sov. Phys. JETP* **54** 64 (1981); *Zh. Eksp. Teor. Fiz.* **81** 132 (1981)
5. Sørensen J L, Hald J, Polzik E S *Phys. Rev. Lett.* **80** 3487 (1998)
6. Mitsui T *Phys. Rev. Lett.* **84** 5292 (2000)
7. Crooker S A et al. *Nature* **431** 49 (2004)
8. Oestreich M et al. *Phys. Rev. Lett.* **95** 216603 (2005)
9. Crooker S A, Cheng L, Smith D L *Phys. Rev. B* **79** 035208 (2009)
10. Römer M et al. *Phys. Rev. B* **81** 075216 (2010)
11. Müller G M et al. *Phys. Rev. Lett.* **101** 206601 (2008)
12. Crooker S A et al. *Phys. Rev. Lett.* **104** 036601 (2010)
13. Li Y et al. *Phys. Rev. Lett.* **108** 186603 (2012)
14. Dahbashi R et al. *Phys. Rev. Lett.* **112** 156601 (2014)
15. Dyakonov M I (Ed.) *Spin Physics in Semiconductors* (Cham: Springer Intern. Publ., 2017)
16. Aleksandrov E B, Zapasskii V S *J. Phys. Conf. Ser.* **324** 012002 (2011)
17. Müller G M et al. *Physica E* **43** 569 (2010)
18. Zapasskii V S *Adv. Opt. Photon.* **5** 131 (2013)
19. Hübner J et al. *Phys. Status Solidi B* **251** 1824 (2014)
20. Sinitsyn N A, Pershin Yu V *Rep. Prog. Phys.* **79** 106501 (2016)
21. Sleator T et al. *Phys. Rev. Lett.* **55** 1742 (1985)
22. Reim W et al. *Phys. Rev. Lett.* **57** 905 (1986)
23. Manassen Y et al. *Phys. Rev. Lett.* **62** 2531 (1989)
24. Durkan C, Welland M E *Appl. Phys. Lett.* **80** 458 (2002)
25. Rugar D et al. *Nature* **430** 329 (2004)
26. Degen C L et al. *Phys. Rev. Lett.* **99** 250601 (2007)
27. Lax M *Rev. Mod. Phys.* **32** 25 (1960)
28. Lax M *Rev. Mod. Phys.* **38** 541 (1966)
29. Gantsevich S V, Gurevich V L, Katilius R *Riv. Nuovo Cimento* **2** 1 (1979)
30. Glazov M M, Ivchenko E L *Phys. Rev. B* **86** 115308 (2012)
31. Glazov M M *J. Appl. Phys.* **113** 136503 (2013)
32. Smirnov D S, Glazov M M *Phys. Rev. B* **90** 085303 (2014)
33. Glazov M M *J. Exp. Theor. Phys.* **122** 472 (2016); *Zh. Eksp. Teor. Fiz.* **149** 547 (2016)
34. Onsager L *Phys. Rev.* **37** 405 (1931)
35. Gorbovitskii P M, Perel' V I *Opt. Spectrosc.* **54** 229 (1983); *Opt. Spektrosk.* **54** 388 (1983)
36. Glazov M M, Zapasskii V S *Opt. Express* **23** 11713 (2015)
37. Cronenberger S, Scalbert D *Rev. Sci. Instrum.* **87** 093111 (2016)
38. Abragam A *The Principles of Nuclear Magnetism* (Oxford: Clarendon Press, 1961); Translated into Russian: *Yadernyi Magnetizm* (Moscow: Ripol Klassik, 2013)
39. Gaudin M *J. Phys. France* **37** 1087 (1976)
40. Yang W, Ma W-L, Liu R-B *Rep. Prog. Phys.* **80** 016001 (2017)
41. Merkulov I A, Efros Al L, Rosen M *Phys. Rev. B* **65** 205309 (2002)
42. Ivchenko E L *Optical Spectroscopy of Semiconductor Nanostructures* (Harrow: Alpha Science, 2005)
43. Urbaszek B et al. *Rev. Mod. Phys.* **85** 79 (2013)
44. Bortz M, Stolze J *J. Stat. Mech.* **6** P06018 (2007)
45. Kozlov G G *J. Exp. Theor. Phys.* **105** 803 (2007); *Zh. Eksp. Teor. Fiz.* **132** 918 (2007)
46. Shumilin A V, Smirnov D S *Phys. Rev. Lett.* **126** 216804 (2021)
47. Glasenapp Ph et al. *Phys. Rev. B* **93** 205429 (2016)
48. Hackmann J, Anders F B *Phys. Rev. B* **89** 045317 (2014)
49. Hackmann J et al. *Phys. Rev. Lett.* **115** 207401 (2015)
50. Hackmann J et al. *Phys. Status Solidi B* **251** 1270 (2014)
51. Braun M, König J *Phys. Rev. B* **75** 085310 (2007)
52. Yue Z, Raikh M E *Phys. Rev. B* **91** 155301 (2015)
53. Poshakinskiy A V, Tarasenko S A *Phys. Rev. B* **101** 075403 (2020)
54. Glasenapp P et al. *Phys. Rev. Lett.* **113** 156601 (2014)
55. Horn H et al. *Phys. Rev. B* **87** 045312 (2013)
56. Kopteva N E et al. *Phys. Rev. B* **100** 205415 (2019)
57. Fröhling N, Anders F B, Glazov M *Phys. Rev. B* **97** 195311 (2018)
58. Landau L D, Lifshitz E M *Quantum Mechanics. Non-Relativistic Theory* (Oxford: Pergamon Press, 1977); Translated from previous Russian ed.: *Kvantovaya Mekhanika* (*Nerelyativistskaya Theoriya*) (Moscow: Fizmatlit, 2004)
59. Dzhioev R I et al. *Phys. Rev. Lett.* **88** 256801 (2002)
60. Dzhioev R I et al. *Phys. Rev. B* **66** 245204 (2002)
61. Smirnov D S, Glazov M M, Ivchenko E L *Phys. Solid State* **56** 254 (2014); *Fiz. Tverd. Tela* **56** 254 (2014)
62. Kavokin K V *Semicond. Sci. Technol.* **23** 114009 (2008)
63. Cronenberger S et al., arXiv:1910.11805
64. Glazov M M *Phys. Rev. B* **91** 195301 (2015)
65. Berski F et al. *Phys. Rev. Lett.* **115** 176601 (2015)
66. Mantsevich V N, Smirnov D S *Phys. Rev. B* **100** 075409 (2019)
67. Ono K et al. *Science* **297** 1313 (2002)
68. Johnson A C et al. *Phys. Rev. B* **72** 165308 (2005)
69. Shumilin A V, Kabanov V V *Phys. Rev. B* **92** 014206 (2015)
70. Parameswaran S A, Vasseur R *Rep. Prog. Phys.* **81** 082501 (2018)
71. Abanin D A et al. *Rev. Mod. Phys.* **91** 021001 (2019)
72. Lifshitz I M *Sov. Phys. Usp.* **7** 549 (1965); *Usp. Fiz. Nauk* **83** 617 (1964)
73. Shklovskii B I, Efros A L *Electronic Properties of Doped Semiconductors* (Berlin: Springer-Verlag, 1984); Translated from Russian: *Elektronnye Svoistva Legirovannykh Poluprovodnikov* (Moscow: Nauka, 1979)
74. Shumilin A V *J. Phys. Condens. Matter* **28** 395301 (2016)
75. Kogan Sh M, Shul'man A Ya *Sov. Phys. JETP* **29** 467 (1969); *Zh. Eksp. Teor. Fiz.* **56** 862 (1969)
76. Kogan Sh *Electronic Noise and Fluctuations in Solids* (Cambridge: Cambridge Univ. Press, 2008)
77. Ivchenko E L *Sov. Phys. Semicond.* **7** 998 (1973); *Fiz. Tekh. Poluprovodn.* **7** 1489 (1973)
78. Gangloff D A et al. *Science* **364** 62 (2019)
79. Smirnov D S *Phys. Rev. B* **91** 205301 (2015)
80. Greilich A et al. *Science* **317** 1896 (2007)
81. Glazov M M, Yugova I A, Efros Al L *Phys. Rev. B* **85** 041303 (2012)
82. Jäschke N, Anders F B, Glazov M M *Phys. Rev. B* **98** 045307 (2018)
83. Poltavtsev S V et al. *Phys. Rev. B* **89** 081304 (2014)
84. Smirnov D S et al. *Phys. Rev. B* **95** 241408 (2017)
85. Astakhov G V et al. *Semicond. Sci. Technol.* **23** 114001 (2008)
86. Kavokin A et al. *Microcavities* (Ser. on Semiconductor Science and Technology, No. 16) (Oxford: Oxford Univ. Press, 2011)
87. Khalfin L A *Sov. Phys. JETP* **6** 1053 (1958); *Zh. Eksp. Teor. Fiz.* **33** 1371 (1957)

88. Facchi P, Pascazio S *J. Phys. A* **41** 493001 (2008)
89. Leppenen N V, Lanco L, Smirnov D S *Phys. Rev. B* **103** 045413 (2021)
90. Misra B, Sudarshan E C G *J. Math. Phys.* **18** 756 (1977)
91. Liu R-B et al. *New J. Phys.* **12** 013018 (2010)
92. Bednorz A, Belzig W, Nitzan A *New J. Phys.* **14** 013009 (2012)
93. Arnold C et al. *Nat. Commun.* **6** 6236 (2015)
94. Smirnov D S et al. *Phys. Rev. B* **96** 165308 (2017)
95. Skalyo J (Jr.) et al. *Phys. Rev. B* **2** 4632 (1970)
96. Dingle R, Lines M E, Holt S L *Phys. Rev.* **187** 643 (1969)
97. Birgeneau R J et al. *Phys. Rev. Lett.* **26** 718 (1971)
98. Hutchings M T et al. *Phys. Rev. B* **5** 1999 (1972)
99. Jordan P, Wigner E *Z. Phys.* **47** 631 (1928)
100. Niemeijer Th *Physica* **36** 377 (1967)
101. Katsura S, Horiguchi T, Suzuki M *Physica* **46** 67 (1970)
102. Sur A, Jasnow D, Lowe I J *Phys. Rev. B* **12** 3845 (1975)
103. Brandt U, Jacoby K *Z. Phys. B* **25** 181 (1976)
104. Capel H W, Perk J H H *Physica A* **87** 211 (1977)
105. Florencio J (Jr.), Lee M H *Phys. Rev. B* **35** 1835 (1987)
106. Luther A, Peschel I *Phys. Rev. B* **12** 3908 (1975)
107. Fogedby H C *J. Phys. C* **11** 4767 (1978)
108. Böhm M et al. *Phys. Rev. B* **49** 15669 (1994)
109. Lifshits I M, Gredeskul S A, Pastur L A *Introduction to the Theory of Disordered Systems* (New York: Wiley, 1988); Translated from Russian: *Vvedenie v Teoriyu Neuporyadochennykh Sistem* (Moscow: Nauka, 1982)
110. Halperin B I *Phys. Rev.* **139** A104 (1965)
111. Berezinskii V L, Gor'kov L P *Sov. Phys. JETP* **50** 1209 (1979); *Zh. Eksp. Teor. Fiz.* **77** 2498 (1979)
112. Berezinskii V L, Gor'kov L P *Sov. Phys. JETP* **51** 409 (1980); *Zh. Eksp. Teor. Fiz.* **78** 812 (1980)
113. Berezinskii V L *Sov. Phys. JETP* **38** 0 (1973); *Zh. Eksp. Teor. Fiz.* **65** 1251 (1973)
114. Gogolin A A *Sov. Phys. JETP* **44** 1003 (1976); *Zh. Eksp. Teor. Fiz.* **71** 1912 (1976)
115. Gogolin A A, Mel'nikov V I, Rashba E I *Sov. Phys. JETP* **42** 168 (1975); *Zh. Eksp. Teor. Fiz.* **69** 327 (1975)
116. Žnidarič M, Prosen T, Prelovšek P *Phys. Rev. B* **77** 064426 (2008)
117. Pal A, Huse D A *Phys. Rev. B* **82** 174411 (2010)
118. Throckmorton R E, Das Sarma S *Phys. Rev. B* **103** 165431 (2021)
119. Shumilin A V, Sherman E Ya, Glazov M M *Phys. Rev. B* **94** 125305 (2016)
120. Dresselhaus G *Phys. Rev.* **100** 580 (1955)
121. Rashba E I, Sheka V I *Fiz. Tverd. Tela* **1** 162 (1959)
122. Bychkov Yu A, Rashba E I *J. Phys. C* **17** 6039 (1984)
123. D'yakonov M I, Kachorovskii V Yu *Sov. Phys. Semicond.* **20** 110 (1986); *Fiz. Tekh. Poluprovodn.* **20** 178 (1986)
124. Averkiev N S, Golub L E *Phys. Rev. B* **60** 15582 (1999)
125. Ganichev D D, Golub L E *Phys. Status Solidi B* **251** 1801 (2014)
126. Glazov M M, Ivchenko E L *JETP Lett.* **75** 403 (2002); *Pis'ma Zh. Eksp. Teor. Fiz.* **75** 476 (2002)
127. Leyland W J H et al. *Phys. Rev. B* **75** 165309 (2007)
128. Gridnev V N *JETP Lett.* **74** 380 (2001); *Pis'ma Zh. Eksp. Teor. Fiz.* **74** 417 (2001)
129. Brand A M et al. *Phys. Rev. Lett.* **89** 236601 (2002)
130. Glazov M M *Solid State Commun.* **142** 531 (2007)
131. Griesbeck M et al. *Phys. Rev. B* **80** 241314 (2009)
132. Gridnev V N *JETP Lett.* **76** 502 (2002); *Pis'ma Zh. Eksp. Teor. Fiz.* **76** 583 (2002)
133. Schliemann J, Carlos Egues J, Loss D *Phys. Rev. Lett.* **90** 146801 (2003)
134. Bernevig B A, Orenstein J, Zhang S-C *Phys. Rev. Lett.* **97** 236601 (2006)
135. Koralek J D et al. *Nature* **458** 610 (2009)
136. Poshakinskiy A V, Tarasenko S A *Phys. Rev. B* **92** 045308 (2015)
137. Passmann F et al. *Semicond. Sci. Technol.* **34** 093002 (2019)
138. Glazov M M, Sherman E Ya, Dugaev V K *Physica E* **42** 2157 (2010)
139. Glazov M M, Sherman E Ya *Phys. Rev. Lett.* **107** 156602 (2011)
140. Li F et al. *Phys. Rev. Lett.* **111** 067201 (2013)
141. Wilamowski Z et al. *Phys. Rev. Lett.* **98** 187203 (2007)
142. Smirnov D S, Golub L E *Phys. Rev. B* **92** 035437 (2015)
143. Vorob'ev L E et al. *Kineticheskie i Opticheskie Yavleniya v Sil'nykh Elektricheskikh Polyakh v Poluprovodnikakh i Nanostrukturakh* (Kinetic and Optical Phenomena in Strong Electric Fields in Semiconductors and Nanostructures) (Eds V I Ul'in, A Ya Shik) (St.Petersburg: Nauka, 2000)
144. D'yakonov M I, Perel' V I *Sov. Phys. Solid State* **13** 3023 (1972); *Fiz. Tverd. Tela* **13** 3581 (1971)
145. Glazov M M et al. *Phys. Rev. B* **88** 041309 (2013)
146. Glazov M M, Kavokin A V *Phys. Rev. B* **91** 161307 (2015)
147. Ryzhov I I et al. *Phys. Rev. B* **93** 241307 (2016)
148. Ryzhov I I et al. *J. Appl. Phys.* **117** 224305 (2015)
149. Kubo R *J. Phys. Soc. Jpn.* **17** 1100 (1962)
150. Mendel J M *Proc. IEEE* **79** 278 (1991)
151. Gardiner C W *Stochastic Methods*: *a Handbook for the Natural and Social Sciences* (Berlin: Springer, 2009)
152. Clerk A A et al. *Rev. Mod. Phys.* **82** 1155 (2010)
153. Kraus K *States, Effects, and Operations*: *Fundamental Notions of Quantum Theory*: *Lectures in Mathematical Physics at the University of Texas at Austin* (Lecture Notes in Physics, Vol. 190, Eds A Böhm, J D Dollard, and W H Wootters) (Berlin: Springer-Verlag, 1983)
154. Aharonov Y, Albert D Z, Vaidman L *Phys. Rev. Lett.* **60** 1351 (1988)
155. Bednorz A et al. *Phys. Rev. Lett.* **110** 250404 (2013)
156. Starosielec S et al. *Rev. Sci. Instrum.* **81** 125101 (2010)
157. Bechtold A et al. *Phys. Rev. Lett.* **117** 027402 (2016)
158. Schad P et al. *Phys. Rev. B* **90** 205419 (2014)
159. Schad P et al. *Ann. Physics* **361** 401 (2015)
160. Li F et al. *New J. Phys.* **15** 113038 (2013)
161. Fröhling N, Anders F B *Phys. Rev. B* **96** 045441 (2017)
162. Fröhling N, Jäschke N, Anders F B *Phys. Rev. B* **99** 155305 (2019)
163. Li F, Sinitsyn N A *Phys. Rev. Lett.* **116** 026601 (2016)
164. Bochkov G N, Kuzovlev Yu E *Physica A* **106** 443 (1981)
165. Sharipova M M et al. *J. Appl. Phys.* **126** 143901 (2019)
166. Li F, Crooker S A, Sinitsyn N A *Phys. Rev. A* **93** 033814 (2016)
167. Fomin A A et al. *Phys. Rev. Res.* **2** 012008 (2020)
168. Smirnov D S, Kavokin K V *Phys. Rev. B* **101** 235416 (2020)
169. Artemova E S, Merkulov I A *Sov. Phys. Solid State* **27** 941 (1985); *Fiz. Tverd. Tela* **27** 1558 (1985)
170. Giri R et al. *Phys. Rev. Lett.* **111** 087603 (2013)
171. Cronenberger S et al. *Nat. Commun.* **6** 8121 (2015)
172. Smirnov D S, Shumilin A V *Phys. Rev. B* **103** 195440 (2021)
173. Ryzhov I I et al. *Appl. Phys. Lett.* **106** 242405 (2015)
174. Ryzhov I I et al. *Sci. Rep.* **6** 21062 (2016)
175. Wiegand J et al. *Phys. Rev. B* **97** 081403 (2018)
176. Wiegand J et al. *Phys. Rev. B* **98** 125426 (2018)
177. Tse W-K et al. *Phys. Rev. Lett.* **113** 046602 (2014)
178. Goryca M et al. *Sci. Adv.* **5** eaau4899 (2019)
179. Ivchenko E L, Pikus G E *JETP Lett.* **27** 604 (1978); *Pis'ma Zh. Eksp. Teor. Fiz.* **27** 640 (1978)
180. Baranova N B, Bogdanov Yu V, Zel'dovich B Ya *Opt. Commun.* **22** 243 (1977)
181. Vorob'ev L E et al. *JETP Lett.* **29** 441 (1979); *Pis'ma Zh. Eksp. Teor. Fiz.* **29** 485 (1979)
182. Smirnov D S, Glazov M M *Phys. Rev. B* **95** 045406 (2017)
183. Ivchenko E L, Spivak B *Phys. Rev. B* **66** 155404 (2002)
184. Kotova L V et al. *Phys. Rev. B* **94** 165309 (2016)
185. Nestoklon M O et al. *Phys. Rev. B* **85** 205307 (2012)
186. Zapasskii V S et al. *Phys. Rev. Lett.* **110** 176601 (2013)
187. Petrov M Yu et al. *Phys. Rev. A* **97** 032502 (2018)
188. Römer M, Hübner J, Oestreich M *Appl. Phys. Lett.* **94** 112105 (2009)
189. Dellis A T, Loulakis M, Kominis I K *Phys. Rev. A* **90** 032705 (2014)
190. Roy D et al. *Sci. Rep.* **5** 9573 (2015)
191. Kozlov G G, Zapasskii V S, Shapochkin P Yu *Appl. Opt.* **57** B170 (2018)
192. Pershin Yu V et al. *Appl. Phys. Lett.* **102** 202405 (2013)
193. Cronenberger S et al. *Phys. Rev. Lett.* **123** 017401 (2019)
194. Kozlov G G, Ryzhov I I, Zapasskii V S *Phys. Rev. A* **95** 043810 (2017)
195. Petrov M Yu et al. *Phys. Rev. B* **97** 125202 (2018)
196. Cronenberger S et al. *Phys. Rev. B* **103** 205208 (2021)
197. Lucivero V G et al. *Phys. Rev. A* **93** 053802 (2016)
198. Li B-B et al. *Optica* **5** 850 (2018)
199. Fischer A et al. *Phys. Rev. B* **102** 165309 (2020)
200. Hägele D, Sifft M, Schefczik F *Phys. Rev. B* **102** 119901 (2020)